Modelling the impact of decidual senescence on embryo implantation in human endometrial assembloids

Thomas M. Rawlings[1,2], Komal Makwana[1,2], Deborah M. Taylor[1,2,3], Matteo A. Molè[4], Katherine J. Fishwick[1], Maria Tryfonos[1,2], Joshua Odendaal[1,5], Amelia Hawkes[1,5], Magdalena Zernicka-Goetz[4,6], Geraldine M. Hartshorne[1,2,3], Jan J. Brosens[1,2,5] and Emma S. Lucas[1,2]

[1]Division of Biomedical Sciences, Warwick Medical School, University of Warwick, Coventry, CV2 2DX, UK.

[2]Centre for Early Life, Warwick Medical School, University of Warwick, Coventry, CV2 2DX, UK.

[3]Centre for Reproductive Medicine, University Hospitals Coventry and Warwickshire NHS Trust, Coventry, CV2 2DX, UK.

[4]Department of Physiology, Development and Neuroscience, University of Cambridge, Downing Street, Cambridge CB2 3EG, UK.

[5]Tommy's National Centre for Miscarriage Research, University Hospitals Coventry & Warwickshire NHS Trust, Coventry, CV2 2DX, UK.

[6]Synthetic Mouse and Human Embryology Group, California Institute of Technology (Caltech), Division of Biology and Biological Engineering, Pasadena, CA 91125, USA.

Corresponding Author: Jan Brosens M.D., Ph.D., Warwick Medical School, University of Warwick, Coventry CV2 2DX, UK. Tel: +44(0)2476968704; FAX: +44(0)2476968653; Email: J.J.Brosens@warwick.ac.uk.

Abstract

Decidual remodelling of midluteal endometrium leads to a short implantation window after which the uterine mucosa either breaks down or is transformed into a robust matrix that accommodates the placenta throughout pregnancy. To gain insights into the underlying mechanisms, we established and characterised endometrial assembloids, consisting of gland organoids and primary stromal cells. Single-cell transcriptomics revealed that decidualized assembloids closely resemble midluteal endometrium, harbouring differentiated and senescent subpopulations in both glands and stroma. We show that acute senescence in glandular epithelium drives secretion of multiple canonical implantation factors, whereas in the stroma it calibrates the emergence of anti-inflammatory decidual cells and pro-inflammatory senescent decidual cells. Pharmacological inhibition of stress responses in pre-decidual cells accelerated decidualization by inhibiting senescence and mesenchymal-epithelial transition, processes involved in endometrial breakdown and regeneration, respectively. Accelerated decidualization resulted in entrapment of co-cultured human blastocysts in a largely static decidual matrix. By contrast, the presence of senescent decidual cells created a dynamic implantation environment, enabling embryo expansion and attachment, although their persistence led to gradual disintegration of assembloids. Our findings demonstrate that senescence controls endometrial fate decisions at implantation and highlight how endometrial assembloids may accelerate the discovery of new treatments to prevent reproductive failure.

Introduction

Upon embryo implantation, the cycling human endometrium transforms into the decidua of pregnancy to accommodate the placenta (Gellersen and Brosens, 2014). Transition between these physiological endometrial states requires intensive tissue remodelling, a process termed decidualization. Notwithstanding that decidualization in early pregnancy cannot be studied directly, a spectrum of prevalent reproductive disorders is attributed to perturbations in this process, including recurrent implantation failure and recurrent pregnancy loss (Dimitriadis et al., 2020, Macklon, 2017, Zhou et al., 2019). By contrast, the sequence of events that renders the endometrium receptive to embryo implantation has been investigated extensively, starting with obligatory estrogen-dependent tissue growth following menstrual repair. As a consequence of rapid proliferation of stromal fibroblasts and glandular epithelial cells, which peaks in the upper third of the functional layer (Ferenczy et al., 1979), endometrial volume and thickness increases multi-fold prior to ovulation (Raine-Fenning et al., 2004, Dallenbach-Hellweg, 1981). After the postovulatory rise in progesterone levels, proliferation of epithelial cells (EpC) first decreases and then ceases altogether in concert with the onset of apocrine glandular secretions, heralding the start of the midluteal window of implantation (Dallenbach-Hellweg, 1981). Concurrently, uterine natural killer (uNK) cells accumulate and endometrial stromal cells (EnSC) start decidualizing in a process that can be described as ‘inflammatory programming’ (Brighton et al., 2017, Chavan et al., 2020, Erkenbrack et al., 2018, Salker et al., 2012). Phenotypic decidual cells emerge upon closure of the 4-day implantation window, meaning that the endometrium has become refractory to embryo implantation (Gellersen and Brosens, 2014). In pregnancy, decidual cells form a robust, tolerogenic matrix in which invading trophoblast cells cooperate with local immune cells to form a haemochorial placenta (Aplin et al., 2020, Vento-Tormo et al., 2018). In non-conception cycles, however, falling progesterone levels and influx of neutrophils leads to breakdown of the superficial endometrial layer and menstrual shedding (Jabbour et al., 2006).

Recently, we highlighted the importance of cellular senescence in endometrial remodelling during the midluteal implantation window (Brighton et al., 2017, Lucas et al., 2020, Kong et al., In press). Senescence denotes a cellular stress response triggered by replicative exhaustion or other stressors that cause macromolecular damage (Munoz-Espin and Serrano, 2014). Activation of tumour suppressor pathways and upregulation of cyclin-dependent kinase inhibitors $p16^{INK4a}$ (encoded by *CDKN2A*) and $p21^{CIP1}$ (*CDKN1A*) lead to permanent cell cycle arrest, induction of survival genes, and production of a bioactive secretome, referred to as the senescence-associated secretory phenotype (SASP). The composition of the SASP is tissue-specific but typically includes proinflammatory and immuno-modulatory cytokines, chemokines, growth factors, and extracellular matrix (ECM) proteins and proteases (Birch and Gil, 2020). Acute senescence, characterised by transient SASP production and rapid immune-mediated clearance of senescent cells, is widely implicated in processes involving physiological tissue remodelling, including during embryo development, placenta formation and wound healing (Munoz-Espin and Serrano, 2014, van Deursen, 2014). By contrast, persisting senescent cells cause chronic inflammation or 'inflammaging' (Birch and Gil, 2020), a pathological state that underpins many age-related disorders. We demonstrated that inflammatory reprogramming of EnSC burdened by replication stress leads to the emergence of acute senescent cells during the implantation window (Brighton et al., 2017, Lucas et al., 2020, Kong et al., In press). Upon successful implantation and continuous progesterone signalling, decidual cells co-opt uNK cells to eliminate their senescent counterparts through granule exocytosis (Brighton et al., 2017, Lucas et al., 2020, Kong et al., In press). Turnover of senescent decidual cells likely promotes recruitment of bone marrow-derived decidual precursor cells, which confer tissue plasticity for rapid decidual expansion in early pregnancy (Diniz-da-Costa et al., In press). Importantly, lack of clonogenic decidual precursor cells and a pro-senescent decidual response are linked to recurrent pregnancy loss (Lucas et al., 2016, Lucas et al., 2020, Tewary et al., 2020).

Based on these insights, we hypothesized that acute senescence is integral to successful implantation, by creating conditions for anchorage of the conceptus in an otherwise tightly adherent decidual matrix. To test this hypothesis, we developed an 'assembloid' model, consisting of endometrial gland organoids and primary EnSC, which recapitulates the complexity in cell states and gene expression of the midluteal implantation window. We used this model to establish co-cultures with human blastocysts and demonstrate that different pathological states associated with implantation failure and miscarriage can be recapitulated in endometrial assembloids by modulating decidual senescence.

Results

Establishment of simple endometrial assembloids

Organoids consisting of gland-like structures are established by culturing endometrial epithelial progenitor cells seeded in Matrigel in a chemically defined medium containing growth factors and signal transduction pathway modulators (Supplementary Table 1) (Turco et al., 2017, Boretto et al., 2017). Gland organoids grown in this medium, termed expansion medium, are genetically stable, easily passaged, and can be maintained in long-term cultures (Boretto et al., 2017, Turco et al., 2017). Estradiol (E2) promotes proliferation of gland organoids and cooperates with NOTCH signalling to activate ciliogenesis in a subpopulation of EpC (Haider et al., 2019). Further, treatment with a progestin (e.g. medroxyprogesterone acetate, MPA) and a cyclic AMP analogue (e.g. 8-bromo-cAMP) induces secretory transformation of gland organoids in parallel with expression of luteal-phase marker genes (Turco et al., 2017).

We modified the gland organoid model to incorporate EnSC. To this end, midluteal endometrial biopsies (Supplementary Table 2) were digested and gland organoids established from isolated EpC (Figure 1A). In parallel, purified EnSC were propagated in standard monolayer cultures. At passage 2, single cell suspensions of EnSC were combined with organoid EpC in a 1:1 ratio (v/v), seeded in hydrogel, and cultured in expansion medium

supplemented with E2 (Figure 1A). The hydrogel matrix comprised 97% type I and 3% type III collagens, which are both present in midluteal endometrium (Oefner et al., 2015, Aplin et al., 1988, Aplin and Jones, 1989, Iwahashi et al., 1996), and has a predicted in-use elastic modulus (Pa) of comparable magnitude to non-pregnant endometrium (Abbas et al., 2019, Bagley, 2019). As shown in Figure 1B, gland formation was unperturbed by the presence of EnSC and assembloids resembled the architecture of native endometrium more closely than organoids. Further, decidualization of assembloids with 8-bromo-cAMP and MPA for 4 days (Figure 1C) resulted in robust secretion of decidual prolactin (PRL) and C-X-C motif chemokine ligand 14 (CXCL14) (Figure 1D). Immunofluorescent microscopy provided further evidence that decidualizing assembloids mimic luteal phase endometrium, exemplified by laminin deposition by decidualizing EnSC, induction of osteopontin (*SPP1*) and accumulation of glycodelin (encoded by *PAEP)* in the lumen of secretory glands, and downregulation of the progesterone receptor (*PGR*) in both stromal and glandular compartments (Figure 1E).

We reasoned that once established assembloids may no longer require exogenous growth factors and pathway modulators for differentiation because of the presence of EnSC. To test this hypothesis, parallel gland organoids and assembloids were established from 3 endometrial biopsies and decidualized with E2, 8-bromo-cAMP and MPA for 4 days in either expansion medium, base medium (Supplementary Table 1), or base medium with each exogeneous factor added back individually. Induction of *PAEP* and *SPP1* was used to monitor the glandular differentiation response. As shown in Figure 2, differentiation of gland organoids in base medium markedly blunted the induction of *PAEP* and *SPP1* when compared to expansion medium. Further, add-back of individual factors did not restore the glandular response. By contrast, addition of N-acetyl-L-cysteine (NAC), a potent antioxidant, to the base medium was sufficient to induce a robust glandular response in assembloids. Thus, in subsequent experiments simple assembloids were grown in expansion medium

supplemented with E2 and then decidualized in minimal differentiation medium (MDM), consisting of base medium containing NAC, E2, 8-bromo-cAMP and MPA.

Cellular complexity of decidualizing assembloids mimics midluteal endometrium

We hypothesized that, depending on the level of replicative stress, individual EpC and EnSC adopt distinct cellular states upon decidualization of endometrial assembloids. Based on previous time-course experiments in 2D cultures, we further speculated that divergence of cells into distinct subpopulations would be apparent by day 4 of differentiation (Brosens et al., 1999, Lucas et al., 2020). To test this hypothesis, we performed single-cell RNA sequencing (scRNA-seq) on undifferentiated assembloids grown for 4 days in expansion medium and assembloids decidualized in MDM for 4 additional days (Figure 3A). Eleven distinct cell clusters were identified by Shared Nearest Neighbour (SNN) and Uniform Manifold Approximation and Projection (UMAP) analysis, segregating broadly into epithelial and stromal populations within the UMAP-1 dimension and into undifferentiated and differentiated subpopulations within the UMAP-2 dimension (Figure 3B). Each cell cluster was annotated based on expression of curated marker genes, which were cross-referenced with a publicly available data set (GEO: GSE4888) to determine their relative expression across the menstrual cycle *in vivo* (Talbi et al., 2006)

We identified five unambiguous EpC subsets. The glandular component of undifferentiated assembloids harboured actively dividing EpC (EpS1; n=198) as well as EpC expressing marker genes of E2-responsive proliferative endometrium (EpS2; n=692), including *PGR* and *CPM* (Figure 3C). EpS3 (n=29) consisted of ciliated EpC, expressing an abundance of genes involved in cilium assembly and organization, including *DNAI1* and *TUBA4B* (Figure 3C). Ciliated cells are the only glandular subpopulation present in both undifferentiated and decidualized assembloids. *In vivo*, EpS3 marker genes transiently peak during the early-luteal phase (Figure 3C). Decidualization of endometrial assembloids led to the emergence of two distinct EpC subsets, EpS4 (n=434) and EpS5 (n=208). Both clusters expressed canonical endometrial 'receptivity genes' (Figure 3C), i.e. genes used in a clinical test to aid

the timing of embryo transfer to the window of implantation in IVF patients (Diaz-Gimeno et al., 2011). In agreement, induction of EpS4 and EpS5 marker genes *in vivo* coincides with the transition from early- to mid-luteal phase. However, while expression of EpS4 marker genes, including *SOD2*, *MAOA* and *PTGS1*, generally peaks during the midluteal window of implantation, EpS5 genes tend to persist or peak during the late-luteal phase (Figure 3C). Additional mining of the data revealed that transition from EpS4 to EpS5 coincides with induction of $p16^{INK4a}$ and $p21^{CIP1}$ in parallel with upregulation of 56 genes encoding secretory factors (Figure 3-figure supplement 1). Notably, several canonical implantation factors secreted by this subpopulation are also well-characterised SASP components, including dipeptidyl peptidase 4 (*DPP4*) (Kim et al., 2017), growth differentiation factor 15 (*GDF15*) (Basisty et al., 2020), and insulin-like growth factor binding protein 3 (*IGFBP3*) (Elzi et al., 2012). Thus, EpS5 consists of senescent EpC producing an implantation-specific SASP.

Decidualized endometrial assembloids also harboured a sizable population of ambiguous cells expressing both epithelial and stromal genes (Figure 3C and Figure 3–figure supplement 2). A hallmark of this subset, termed 'transitional population' (TP; n=472), is the induction of long non-coding RNAs involved in mesenchymal-epithelial and epithelial-mesenchymal transition (MET/EMT), such as *NEAT1* (nuclear paraspeckle assembly transcript 1) and *KCNQ1OT1* (KCNQ1 opposite strand/antisense transcript 1) (Bian et al., 2019, Chen et al., 2021). GO analysis showed that both EpS5 and the transitional population are comprised of secretory cells involved in ECM organization (Figure 3D). However, while EpS5 genes are implicated in neutrophil activation (a hallmark of premenstrual endometrium), genes expressed by the transitional population are uniquely enriched in GO terms such as 'wound healing', 'regulation of stem cell proliferation', 'blood coagulation' and 'blood vessel development' (Figure 3D), which points towards a putative role in tissue repair and regeneration.

The stromal fraction of undifferentiated assembloids consisted of actively dividing EnSC (stromal subpopulation 1 [SS1]; n=434) and E2-responsive EnSC (SS2; n=874) expressing

proliferative phase marker genes, such as *PGR*, *MMP11*, *and CRABP2* (Figure 3E). As anticipated, decidualization of assembloids for 4 days led to a preponderance of pre-decidual cells (SS3; n=495) as well as emerging decidual cells (SS4; n=87) and senescent decidual cells (SS5; n=118) (Figure 3E). Each of these subpopulations expressed marker genes identified previously by scRNA-seq reconstruction of the decidual pathway in standard primary EnSC cultures (Lucas et al., 2020). Pre-decidual cells in SS3 express *HAND2*, a key decidual transcription factor (Marinic et al., 2021), as well as previously identified genes encoding secreted factors, including *VEGFA* (vascular endothelial growth factor A), *CRISPLD2* (a progesterone-dependent anti-inflammatory response gene coding cysteine rich secretory protein LCCL domain containing 2)*, IL15* (interleukin 15) and *TIMP3* (TIMP metallopeptidase inhibitor 3) (Lucas et al., 2020). Novel pre-decidual genes were also identified, such as *DDIT4* (DNA damage inducible transcript 4), encoding a stress response protein intimately involved in autophagy, stemness and antioxidative defences (Ho et al., 2020, Miller et al., 2020). Decidual cells (SS4) and senescent decidual cells (SS5) express *SCARA5* and *DIO2*, respectively (Figure 3E), two stroma-specific marker genes identified by scRNA-seq analysis of mid- and late-luteal endometrial biopsies (Lucas et al., 2020). SS3 and SS4 genes mapped to the early- and mid-luteal phase of the cycle whereas SS5 genes peak in the late-luteal phase, i.e. prior to menstrual breakdown. Notably, the transcriptomic profiles of SS3 and SS5 are enriched in GO terms such as 'Wound healing', 'Response to hypoxia', and 'Inflammatory response', suggesting that both clusters comprise stressed cells (Figure 3F). However, the nature of the cellular stress response differs between these populations with only senescent decidual cells (SS5) expressing genes enriched in categories such as 'Embryo implantation' 'Cellular senescence', 'Aging', and 'Leukocyte activation'. By contrast, few notable categories were selectively enriched in decidual cells (e.g. 'Mesenchymal cell differentiation'), rendering the lack of GO terms that pertain to stress, inflammation, or wound healing perhaps the most striking observation. In keeping with the GO analysis, senescent decidual cells (SS5) express a multitude of SASP-related genes (Figure 3-figure supplement 3), including matrix metallopeptidases (e.g. *MMP3*, *7*, *9*,

10, *11* and *14*), insulin-like growth factor binding proteins (e.g. *IGFBP1*, *3*, *6* and *7*), growth factors (e.g. *AREG*, *FGF2*, *FGF7*, *HGF*, *PDGFRA*, *PDGFRB*, and *VEGFA*), cytokines (e.g. *LIF*, *IL6*, *IL1A*, and *IL11*), chemokines (e.g. *CXCL8* and *CXCL1*), and members of the TGF-β superfamily of proteins (e.g. *GDF15*, *INHBA*, and *BMP2*). By contrast, decidual cells are characterised by expression of an unique network of secretory genes, some encoding ECM proteins (e.g. *COL1A1*, *COL3A1*, and *LAMA4*) and others known decidual markers (e.g. *PRL*, *PROK1* and *WNT4*) as well as factors involved in uNK cell chemotaxis and activation (e.g. *CCL2*, *CXCL14*, and *IL15*) (Figure 3-figure supplement 3).

Taken together, single-cell analysis of undifferentiated and decidualized assembloids revealed a surprising level of cellular complexity. Each epithelial and stromal subpopulation appears functionally distinct and maps to a specific phase of the menstrual cycle. Transition between cellular states is predicated on changes in cell cycle status, ranging from actively dividing cells in proliferating assembloids to the emergence upon differentiation of highly secretory senescent epithelial and decidual subpopulations, resembling premenstrual endometrium. However, the dominant subpopulations on day 4 of decidualization are EpS4 and SS3, which map to the midluteal implantation window *in vivo*.

Receptor-ligand interactions in decidualizing assembloids

We used CellPhoneDB to explore putative interactions between subpopulations in decidualizing assembloids. This computational tool takes into account the subunit architecture of both ligands and receptors in heteromeric complexes (Efremova et al., 2020, Vento-Tormo et al., 2018). The number of predicted interactions is depicted in Figure 4A, showing a conspicuous lack of crosstalk between the transitional population and any other populations. Conversely, the most abundant interactions centre around the secretory subpopulations, EpC5 and SS5.

A total of 270 significantly enriched (non-integrin) receptor-ligand interactions (FDR-corrected $P < 0.05$) were identified between epithelial and stromal subsets in decidualizing

assembloids (Figure 4-Source Data 1), a representative selection of which are shown in Figures 4B. Within the multitude of predicted complex interactions, three broad categories can be discerned. First, there are non-selective interactions involving ligands produced by all subpopulations in one compartment acting on receptors expressed by all subsets in the other compartment. Second, there are semi-selective stromal-epithelial interactions involving 3 or 4 subpopulations across both compartments. For example, binding of WNT5A secreted by all decidual stromal subsets to FZD3 (frizzled class receptor 3) expressed on all epithelial cells represents a non-selective receptor-ligand interaction whereas binding of WNT5A or WNT4 to FZD6 is a predicted semi-selective interaction, involving all stromal subsets (SS3-5) and EpS4 but not EpS5 (Figure 4B). While FZD3 activates the canonical β–catenin pathway, FZD6 functions as a negative regulator of this signalling cascade (Corda and Sala, 2017). Finally, we identified only three highly-selective receptor-ligand interactions (Figure 4B), two of which involved secretion of decidual ligands, prolactin (PRL) and C-X-C motif chemokine ligand 12 (CXCL12), acting on their cognate receptors expressed on receptive EpC (EpC4). CXCL12-dependent activation of C-X-C motif chemokine receptor 4 (CXCR4) has been shown to promote motility of EpC (Zheng et al., 2020); whereas PRL is a lactogenic hormone that stimulates glandular secretion in early pregnancy (Burton et al., 2020).

In contrast to stromal-epithelial communication, non-selective interactions are predicted to be rare between decidual subsets. Instead, communication appears governed largely by a combinatorial network of receptor-ligand interactions (Figure 4C). For example, colony stimulating factor 3 (CSF3) and vascular endothelial growth factor A (VEGFA) produced by senescent decidual cells (SS5) is predicted to impact selectively on pre-decidual cells (SS3) whereas secretion of inhibin A (INHBA) may engage both pre-decidual and decidual cells (SS4). Other interactions are predicted to govern crosstalk between SS3 and SS4, such as modulation of the WNT pathway in response to binding of R-spondin 3 (RSPO3) to leucine-rich repeat-containing G protein-coupled receptor 4 (LGR4). A striking observation is the

overrepresentation of receptor tyrosine kinases implicated in SS3 and SS5 signal transduction as well as the involvement of receptors that signal through downstream cytoplasmic tyrosine kinases, including CSF3 receptor (CSF3R) and CD44 (Figure 4C) (Corey et al., 1998, van der Voort et al., 1999).

Tyrosine kinase-dependent stress responses determines the fate of decidual cells

The CellPhoneDB analysis inferred that epithelial-stromal crosstalk in assembloids is robust, buffered by numerous non-selective interactions, whereas decidual subsets are reliant on selective receptor-ligand interactions and activation of distinct signal transduction pathways. For example, the predicted tyrosine kinase-dependency of pre-decidual (SS3) and senescent decidual cells (SS5) raised the possibility that these subpopulations can be targeted by tyrosine kinase inhibitors, such as dasatinib (Brighton et al., 2017, Zhu et al., 2015). To test this supposition, we generated single-cell transcriptomic profiles of assembloids decidualized for 4 days in the presence of dasatinib (Figure 5A). We found that tyrosine kinase inhibition upon decidualization had a dramatic impact on stromal subpopulations, virtually eliminating senescent decidual cells (SS5, n=7) and increasing the abundance of decidual cells 9-fold (SS4, n=882) (Figure 5B). Apart from a modest reduction in pre-decidual cells (SS3), dasatinib also impacted markedly on transitional cells, reducing their numbers by 76%. By contrast, the effect on epithelial populations was confined to a modest reduction in senescent EpC (EpS5) (Figure 5B). Further, relatively few genes were perturbed significantly (FDR-corrected $P < 0.05$) upon dasatinib treatment in epithelial populations (Figure 5C). In the stroma, dasatinib triggered a conspicuous transcriptional response in pre-decidual (SS3) and transitional cells, whereas gene expression in decidual cells (SS4) and the few remaining senescent decidual cells (SS5) was largely unaffected (Figure 5C). In transitional cells, dasatinib simultaneously upregulated genes encoding canonical mesenchymal markers (e.g. *SNAI2*, *TWIST2*, *ZEB1*, *COL1A1*, and *FBN1*) (Owusu-Akyaw et al., 2019) and decidual factors (e.g. *SCARA5*, *FOXO1*, *GADD45A*, *IL15*, *CXCL14*, and *SGK1*) (Gellersen and Brosens, 2014), revealing that MET accounts for the

emergence of this population upon decidualization (Figure 5-Source Data 1). In pre-decidual cells, dasatinib inhibited the expression of a network of genes enriched in GO categories such as 'Response to wounding' (FDR-corrected $P = 3.5 \times 10^{-5}$), 'Response to stress' (FDR-corrected $P = 3.8 \times 10^{-5}$), and 'Response to oxidative stress' (FDR-corrected $P = 1.3 \times 10^{-4}$), indicative of a blunted stress response. To substantiate this finding, we measured the secreted levels of CXCL8 (IL-8), a potent inflammatory mediator implicated in autocrine/paracrine propagation of cellular senescence (Acosta et al., 2008, Kuilman et al., 2008), in assembloids decidualized with or without dasatinib. CXCL14, IL-15, and TIMP3 levels were also measured to monitor the decidual response. As shown in Figure 5D, dasatinib completely abrogated the release of CXCL8 by pre-decidual cells while markedly enhancing subsequent secretion of CXCL14, IL-15, and TIMP3, which are involved in effecting immune clearance of senescent decidual cells (Brighton et al., 2017, Lucas et al., 2020, Kong et al., In press). Together, these observations not only support the CellPhoneDB predictions but also indicate that the amplitude of the cellular stress response during the pre-decidual phase determines the subsequent decidual trajectory, with low levels accelerating differentiation and high levels promoting cellular senescence and MET.

Modelling the impact of decidual subpopulations on human embryos.

We postulated that decidual invasion by human embryos that have breached the luminal endometrial epithelium depends on an acute cellular senescence and transient SASP production, rich in growth factors and proteases. Conversely, we reasoned that lack of senescent decidual cells or unconstrained SASP should simulate pathological implantation environments associated with implantation failure and early pregnancy loss, respectively. To test this hypothesis, we constructed a simple implantation model by embedding human embryos in endometrial assembloids. To this end, assembloids were first decidualized for 96 hours in the presence or absence of dasatinib, washed and cultured in embryo medium, consisting of MDM with added supplements (Figure 6A and Supplementary Table 1). Day 5 human blastocysts were placed into small pockets created in the decidualized assembloids

(Figure 6B) and individual embryo-assembloid co-cultures imaged using time-lapse microscopy over 72 hours. Co-cultured blastocysts (n=4) expanded markedly when placed in decidualized assembloids that were not pre-treated with dasatinib (Figure 6C and D). Time-lapse microscopy revealed intense cellular movement in the stromal compartment as well as evidence that interaction between migratory decidual cells and polar trophectoderm promotes adherence and early invasion of the embryo (Video 1). Upon retrieval and processing, we were able to identify proliferating polar trophectoderm in one firmly attached embryo as well as expression of OCT4 and GATA6 in the epiblast and hypoblast, respectively (Figure 6E). A major limitation of this implantation model is that persistence of senescent decidual cells also causes gradual disintegration of the assembloids (Figure 6–figure supplement 1). By contrast, pre-treatment with dasatinib, which accelerates decidualization and all but eliminates decidual senescence, resulted in much more robust assembloids. However, all embedded blastocysts (n=4) failed to expand in this model (Figure 6C and D). Further, movement of the decidual matrix was greatly reduced and directed migration or attachment of decidual cells to the blastocyst was not observed (Video 2). Secreted levels of human chorionic gonadotropin (hCG) did not differ between co-cultures (Figure 6E), indicating that all embryos remained viable over the 72-hour observation period. Thus, while our experimental design precluded modelling of physiological embryo implantation, different pathological endometrial states underlying reproductive failure were recapitulated in simple assembloids.

Discussion

There is ample clinical evidence that insufficient endometrial growth decreases the likelihood of successful embryo implantation (Kasius et al., 2014), although the underlying reasons are less clear. Following menstruation, E2-dependent proliferation of both glandular EpC and EnSC accelerates with increasing distance from the endometrial-myometrial interface (Ferenczy et al., 1979), a response linked to presence of an IFN-γ gradient generated by lymphoid aggregates residing in the basal endometrial layer (Christian et al., 2001,

Tabibzadeh, 1991, Tabibzadeh et al., 1993). Stromal remodelling and secretory transformation of the glands during the luteal phase are also confined to the superficial endometrial layer, indicating that rapid proliferation is intricately linked to the post-ovulatory differentiation responses, cumulating in a midluteal implantation window. Our single-cell analysis of simple endometrial assembloids provides compelling evidence that the sequence of events leading up to the implantation window, and beyond, requires divergence of both glandular EpC and EnSC into differentiated and senescent subpopulations, a process likely determined by the level of replication stress incurred by individual cells in the preceding proliferative phase (Brighton et al., 2017). Importantly, we demonstrate that acute senescence in glandular EpC (EpS5) underpins production of an implantation-specific SASP, comprising canonical implantation factors and growth factors, such as amphiregulin (*AREG*) and epiregulin (*EREG*), implicated in transforming cytotrophoblasts into extravillous trophoblasts (Cui et al., 2020, Yu et al., 2019). On the other hand, the transcriptome profile of differentiated EpC (EpS4) revealed a pivotal role for this subpopulation in prostaglandin and glycodelin synthesis. Prostaglandins, and specifically PGE2, are indispensable for implantation (Ruan et al., 2012), whereas glycodelin is an abundantly secreted, multifaceted glycoprotein involved in blastocyst attachment, trophoblast differentiation, and immune modulation in early pregnancy (Lee et al., 2016). Further, differentiated EpC highly express *SLC2A1*, encoding the major glucose transporter GLUT1. Glucose is required for glycogen synthesis, an essential component of glandular secretions that nourishes the conceptus prior to the onset of placental perfusion around 10 weeks of pregnancy (Burton et al., 2020). The fate and function of senescent EpC in pregnancy is unknown. Arguably, localised secretion of proteinases by senescent EpC may promote breakdown of the surrounding basement membrane, thereby facilitating endoglandular trophoblast invasion and access to histotrophic nutrition in early gestation (Huppertz, 2019, Moser et al., 2010). In non-conception cycles, the abundance of $p16^{INK4}$-positive glandular EpC rises markedly during the late-luteal phase (Brighton et al., 2017), indicating that senescent EpC are progesterone-

independent and likely responsible for glandular breakdown in the superficial endometrial layer at menstruation.

Decidual transformation of EnSC in assembloids unfolded largely as anticipated from previous studies, i.e. starting with an acute pre-decidual stress response and leading to the emergence of both decidual and senescent decidual subpopulations (Brighton et al., 2017, Lucas et al., 2020, Kong et al., In press). Like their epithelial counterparts, senescent decidual cells have a conspicuous secretory phenotype. We identified 56 and 72 genes encoding secreted factors upregulated in senescent epithelial and decidual subpopulations, respectively. However, only 15 genes were shared, indicating that the SASP generated in both cellular compartments is distinct. As glandular secretions drain into the uterine cavity, the embryonic microenvironment is therefore predicted to change abruptly upon breaching of the luminal epithelium. Based on computational predictions of ligand-receptor interactions, we demonstrated that the decidual response in the stroma can be targeted pharmacologically with only modest impact on glandular function and, by extension, the preimplantation embryo milieu. Specifically, dasatinib, a tyrosine kinase inhibitor, was highly effective in blunting the pre-decidual stress response, leading to a dramatic expansion of anti-inflammatory decidual cells and near-total elimination of senescent decidual cells. Dasatinib also inhibited MET and shifted the transcriptional profile of the remaining transitional cells towards a decidual phenotype. An analogous population of ambiguous cells expressing both epithelial and mesenchymal marker genes was recently identified in midluteal endometrium by scRNA-seq analysis (Lucas et al., 2020). Further, based on CellPhoneDB and GO analyses, decidualization-associated EpC are predicted to be highly autonomous and involved in tissue regeneration, in line with experimental evidence that MET drives re-epithelization of the endometrium following menstruation and parturition (Owusu-Akyaw et al., 2019, Patterson et al., 2013). Thus, the level of endogenous cellular stress generated by the endometrium during the window of implantation calibrates the subsequent decidual trajectory, either promoting the formation of a robust decidual matrix or

facilitating tissue breakdown and repair. Further, an in-built feature of both trajectories is self-enforcement, as decidual cells recruit and activate uNK cells to eliminate their senescent counterparts (Brighton et al., 2017, Lucas et al., 2020, Kong et al., In press), whereas senescent decidual cells induce secondary senescence in neighbouring decidual (Brighton et al., 2017, Ozaki et al., 2017) and, plausibly, uNK cells (Rajagopalan and Long, 2012) .

Clinically, recurrent pregnancy loss, defined as multiple miscarriages, is associated with loss of endometrial clonogenicity (Lucas et al., 2016, Diniz-da-Costa et al., In press), uNK cell deficiency and excessive decidual senescence (Lucas et al., 2020, Tewary et al., 2020), and rapid conceptions (also referred to as 'superfertility') (Dimitriadis et al., 2020, Ticconi et al., 2020). Conversely, lack of a proliferative gene signature in midluteal endometrium and premature expression of decidual PRL have been linked to recurrent implantation failure (Berkhout et al., 2020b, Koler et al., 2009, Koot et al., 2016), a pathological condition defined by a failure to achieve a pregnancy following transfer of one or more high-quality embryos in multiple IVF cycles (Polanski et al., 2014). We reasoned that these aberrant implantation environments can be recapitulated in assembloids by manipulating the level of decidual senescence. In line with these predictions, the presence of senescent decidual cells created a permissive environment in which migratory decidual cells interacted with expanding blastocysts, although continuous SASP production also promoted breakdown of the assembloids. Conversely, in the absence of senescent decidual cells, non-expanding embryos became entrapped in a robust but stagnant decidual matrix. These observations are in keeping with previous studies demonstrating that implantation of human embryos depends critically on the invasive and migratory capacities of decidual cells (Berkhout et al., 2020a, Gellersen et al., 2010, Grewal et al., 2008, Weimar et al., 2012). Our co-culture experiments also highlighted the shortcomings of simple assembloids as an implantation model, including the lack of a surface epithelium to create distinct pre- and post-implantation

445 microenvironments and the absence of key cellular constituents, such as innate immune
446 cells.

447 In summary, parsing the mechanisms that control implantation has been hampered by the
448 overwhelming complexity of factors involved in endometrial receptivity. Our single-cell
449 analysis of decidualizing assembloids suggests that this complexity reflects the reliance of
450 the human endometrium on rapid E2-dependent proliferation and replicative exhaustion to
451 generate both differentiated and senescent epithelial and stromal subpopulations in
452 response to the postovulatory rise in progesterone. We demonstrate that senescent cells in
453 both cellular compartments produce distinct bioactive secretomes, which plausibly prime
454 pre-implantation embryos for interaction with the luminal epithelium and then stimulate
455 encapsulation by underlying decidual stromal cells. Based on our co-culture observations,
456 we predict that a blunted pre-decidual stress response causes implantation failure because
457 of a lack of senescence-induced tissue remodelling and accelerated decidualization.
458 Conversely, a heightened stress response leading to excessive decidual senescence may
459 render embryo implantation effortless, albeit in a decidual matrix destined for breakdown and
460 repair. Finally, we demonstrated that pre-decidual stress responses can be modulated
461 pharmacologically, highlighting the potential of endometrial assembloids as a versatile
462 system to evaluate new or repurposed drugs aimed at preventing reproductive failure.

Materials and Methods

Ethical approvals, endometrial samples and human blastocysts

Endometrial biopsies were obtained from women attending the Implantation Research Clinic, University Hospitals Coventry and Warwickshire National Health Service Trust. Written informed consent was obtained in accordance with the Declaration of Helsinki 2000. The study was approved by the NHS National Research Ethics Committee of Hammersmith and Queen Charlotte's Hospital NHS Trust (1997/5065) and Tommy's Reproductive Health Biobank (Project TSR19-002E, REC Reference: 18/WA/0356). Timed endometrial biopsies were obtained 6 to 11 days after the post-ovulatory LH surge using a Wallach Endocell™ Endometrial Cell Sampler. Patient demographics for the samples used in each experiment are detailed in Supplementary Table 2.

The use of vitrified human blastocysts was carried out under a Human Fertilisation and Embryology Authority research licence (HFEA: R0155) with local National Health Service Research Ethics Committee approval (04/Q2802/26). Spare blastocysts were donated to research following informed consent by couples who had completed their fertility treatment at the Centre for Reproductive Medicine, University Hospitals Coventry and Warwickshire National Health Service Trust. Briefly, women underwent ovarian stimulation and oocytes were collected by transvaginal ultrasound-guided aspiration and inseminated with prepared sperm (day 0). All oocytes examined 16-18 hours after insemination and classified as normally fertilised were incubated under oil in 20-25 µL drops of culture media (ORIGIO Sequential Cleav and Blast media, CooperSurgical, Denmark) at 5 % O_2, 6 % CO_2, 89% N_2 at 37°C. Following culture to day 5 of development, the embryo(s) with the highest quality was selected for transfer, whereas surplus embryos considered top-quality blastocysts were cryopreserved on day 5 or 6 by vitrification using Kitazato vitrification media (Dibimed, Spain) and stored in liquid nitrogen. Prior to their use in the co-culture, vitrified blastocysts were warmed using the Kitazato vitrification warming media (Dibimed, Spain) and underwent zona pellucida removal using a Saturn 5 Laser (CooperSurgical, Denmark). Blastocysts

were then incubated for 1 hour under oil in 20 µL drops of culture media (ORIGIO Sequential Blast media, CooperSurgical, Denmark) at 5 % O_2, 6 % CO_2, 89% N_2 at 37°C and allowed to re-expand.

Processing of endometrial biopsies and primary EnSC cultures.

Unless otherwise stated, reagents were obtained from Life Technologies (Paisley, UK). Cell cultures were incubated at 37°C, 5% CO_2 in a humidified incubator. Centrifugation and incubation steps were performed at room temperature unless stated otherwise. Fresh endometrial biopsies were processed as described previously (Barros et al., 2016). Briefly, tissue was finely minced for 5 minutes using a scalpel blade. Minced tissue was then digested enzymatically with 0.5 mg/ml collagenase I (Sigma Aldrich, Gillingham, UK) and 0.1 mg/ml deoxyribonuclease (DNase) type I (Lorne Laboratories, Reading, UK) in 5 ml phenol red-free Dulbecco's Modified Eagle Medium (DMEM)/F12 for 1 hour at 37°C, with regular vigorous shaking. Dissociated cells were washed with growth medium [DMEM/F12 containing 10% dextran-coated charcoal stripped FBS (DCC-FBS), 1% penicillin-streptomycin, 2 mM L-glutamine, 1 nM E2 (Sigma Aldrich) and 2 mg/ml insulin (Sigma Aldrich)]. Samples were passed through a 40-µm cell sieve. EnSC were collected from the flow-through, while epithelial clumps remained in the sieve and were collected by backwashing into a 50 ml Falcon tube. Samples were resuspended in growth medium and centrifuged at 400 $\times$ *g* for 5 minutes. EnSC pellets were resuspended in 10 ml growth medium and plated in tissue culture flasks. To isolate EnSC from other (non-adherent) cells collected in the flowthrough, medium was refreshed after 24 hours. Thereafter, medium was refreshed every 48 hours. Sub-confluent monolayers were passaged using 0.25% Trypsin-EDTA and split at a ratio of 1:3.

Endometrial gland organoid culture

Endometrial gland organoids were established as described previously (Turco et al., 2017), with adaptations. Freshly isolated endometrial gland fragments were resuspended in 500 µl

phenol red-free DMEM/F12 medium in a microcentrifuge tube and centrifuged at 600 × *g* for 5 minutes. The medium was aspirated and ice-cold, growth factor-reduced Matrigel® (Corning Life Sciences B.V., Amsterdam, Netherlands) was added at a ratio of 1:20 (cell pellet: Matrigel®). Samples mixed in Matrigel® were kept on ice until plating at which point the suspension was aliquoted in 20 µl volumes to a 48 well plate, one drop per well, and allowed to cure for 15 minutes. Expansion medium supplemented with E2 (Supplementary Table 1) (Turco et al., 2017) was then added and samples cultured for up to 7 days. For passaging, Matrigel® droplets containing gland organoids were collected into microcentrifuge tubes and centrifuged at 600 × *g* for 6 minutes at 4^{o}C. Samples were resuspended in ice-cold, phenol red-free DMEM/F12 and subjected to manual pipetting to disrupt the organoids. Suspensions were centrifuged again, resuspended in ice cold additive free DMEM/F12 and then subjected to further manual pipetting. Suspensions were centrifuged again and either resuspended in Matrigel® and plated as described above for continued expansion or used to establish assembloid cultures.

Establishment of assembloid cultures

At passage 2, EnSC and gland organoid pellets were mixed at a ratio of 1:1 (v/v) and ice-cold PureCol® EZ Gel (Sigma Aldrich) added at a ratio of 1:20 (cell pellet: hydrogel). Samples were kept on ice until plating. The suspension was aliquoted in 20 µl volumes using ice-cold pipette tips into a 48-well plate, one droplet per well, and allowed to cure in the cell culture incubator for 45 minutes. Expansion medium supplemented with 10 nM E2 was overlaid and the medium was refreshed every 48 hours. For decidualization experiments, assembloid cultures were grown in expansion medium supplemented with E2 for 4 days to allow for growth and expansion. Assembloids were then either harvested or decidualized using different media as tabulated in Supplementary Table1 for a further 4 days. Again, the medium was refreshed every 48 hours and spent medium stored for further analysis. For tyrosine kinase inhibition, MDM was supplemented with 250 nM dasatinib (Cell Signaling Technology, Leiden, NL).

Fluorescence microscopy

For fluorescent microscopy, assembloids were removed from culture wells and transferred into tubes for fixation. Samples were washed in PBS and fixed in 10% neutral buffered formalin in the tube for 15 minutes, then washed three times with PBS and stored for use. Samples were dehydrated in increasing concentrations of ethanol (70% then 90% for 1 hour each, followed by 100% for 90 minutes), then incubated in xylene for 1 hour. After paraffin wax embedding, 5 µm sections were cut and mounted, then incubated overnight at 60 °C. Slides were then stored at 4°C until further processing. De-paraffinization and rehydration were performed through xylene, 100% isopropanol, 70% isopropanol and distilled water incubations. Following antigen retrieval, permeabilization was performed where appropriate by incubation with 0.1% Triton X-100 for 30 minutes. Slides were then washed, blocked, and incubated in primary antibodies overnight at 4°C. Antibody details are presented in Supplementary Table 3. After washing three times, slides were incubated with secondary antibodies for 2 hours, then washed as before and mounted in ProLong Gold® Antifade Reagent with DAPI (Cell Signaling Technology). Slides were visualised using the EVOS Auto system, with imaging parameters maintained throughout image acquisition. Images were merged in ImageJ and any adjustments to brightness or contrast were applied equally within comparisons.

Real-time quantitative polymerase chain reaction

After removal of spent medium, gland organoid cultures were washed in PBS and harvested in 200 µl Cell Recovery Solution (Corning). Gel droplets were transferred to nuclease-free microcentrifuge tubes and placed at 4°C for 30 minutes. Samples were then washed in PBS, centrifuged at 600 × *g* for 6 minutes twice and snap frozen as cell pellets. Assembloid cultures were washed with PBS and then recovered by directly scraping the samples into nuclease-free microcentrifuge tubes. Samples were centrifuged at 600 × *g* for 6 minutes. The cellular pellet was resuspended in 500 µl of 500 µg/ml collagenase I diluted in additive-

free DMEM/F12 and incubated at 37°C for 10 minutes with regular manual shaking. Samples were washed twice in PBS, with centrifugation at 600 × *g* for 6 minutes, then cell pellets were snap frozen. RNA extraction was performed using the RNeasy Micro Kit (QIAGEN, Manchester, UK) according to manufacturer's instructions. RNA concentration and purity were determined using a NanoDrop ND-1000. All RNA samples were stored at -80°C until use. Reverse transcription was performed using the QuantiTect Reverse Transcription (RT) Kit according to manufacturer's protocol (QIAGEN). Input RNA was determined by the sample with lowest concentration within each experiment. Genes of interest were amplified using PrecisionPlus SYBR Green Mastermix (PrimerDesign, Southampton, UK). Amplification was performed in 10 µl reactions containing 5µl PrecisionPlus 2× master mix, 300nM each of forward and reverse primer, nuclease free water and 1µl of cDNA or water control. Amplification was performed for 40 cycles on an Applied Biosystems QuantStudio 5 Real-Time PCR System (qPCR). Data were analysed using the Pffafl method (Pfaffl, 2001) and *L19* was used as a reference gene. Primer sequences were as follows: *L19* forward: 5'-GCG GAA GGG TAC AGC CAA T-3', *L19* reverse: 5'-GCA GCC GGC GCA AA-3', *PAEP* forward: 5'-GAG CAT GAT GTG CCA GTA CC-3', *PAEP* reverse: 5'-CCT GAA AGC CCT GAT GAA TCC-3', *SPP1* forward: 5'-TGC AGC CTT CTC AGC CAA A-3', *SPP1* reverse: 5'-GGA GGC AAA AGC AAA TCA CTG-3'.

Enzyme-linked immunosorbent assay

Spent medium was collected every two days during a 4-day decidual time course, with or without dasatinib treatment. Duoset solid phase sandwich enzyme-linked immunosorbent assay (ELISA) kits (Bio-Techne, Abingdon, UK) were used for the detection of PRL (DY682), TIMP3 (DY973), IL-8 (DY208), IL-15 (DY247), CXCL14 (DY866) and HCG (DY9034). Assays were performed according to manufacturer's instructions. Absorbance at 450 nm was measured on a PheraStar microplate reader (BMG LABTECH Ltd, Aylesbury, UK), with background subtraction from absorbance measured at 540 nm. Protein concentration was obtained using a 4-parameter logistic regression analysis and interpolation from the curve.

Single-cell capture, library preparation and sequencing

Assembloids were dissociated to single cells by incubation of gel droplets with 0.5 mg/ml Collagenase I for 10 minutes in a 37°C water bath for 10 minutes with regular vigorous shaking. Samples were washed with additive free DMEM/F12 phenol free medium and incubated with 5×TrypLE Select diluted in additive free DMEM/F12 phenol free medium for 5 minutes in a 37°C water bath. Cell clumps were disrupted by manual pipetting, then suspended in 0.1% BSA in PBS and passed through a 35 µm cell sieve. Droplet generation was performed using a Nadia Instrument (Dolomite Bio, Cambridge, UK) according to the manufacturer's guidelines and using reagents as described by Macosko et al., (2015) and the scRNAseq v1.8 protocol (Dolomite Bio). Pooled beads were processed as described previously (Lucas et al., 2020) and sequenced using a NextSeq 500 with high output 75 cycle cartridge (Illumina, Cambridge, UK) by the University of Warwick Genomics Facility.

Bioinformatics analysis

Initial single cell RNAseq data processing was performed using Drop-Seq_tools-2.3.0 (DropseqAlignmentCookbook_v2Sept2018, http://mccarrolllab.com/dropseq) and as described previously (Lucas et al., 2020). To select high-quality data for analysis, cells were included when at least 200 genes were detected, while genes were included if they were detected in at least 3 cells. Cells with more than 5000 genes were excluded from the analysis as were cells with more than 5 % mitochondrial gene transcripts, to minimize doublets and low quality (broken or damaged) cells, respectively. The Seurat v3 standard workflow (Stuart et al., 2019) was used to integrate datasets from biological replicates. Clustering and nearest neighbour analysis was performed on the full integrated dataset using principle components 1:15 and a resolution of 0.6. The 'subset' function was applied for interrogation of specific experimental conditions and timepoints. Gene ontology (GO) analysis was performed on differentially expressed genes from specified 'FindMarkers' comparisons in Seurat v3 using the Gene Ontology Consortium database (Ashburner et al., 2000, The Gene Ontology, 2019, Mi et al., 2013). Dot plots of significantly enriched GO

terms (FDR adjusted $P < 0.05$) were generated in RStudio (version 1.2.5042). CellPhoneDB was used to predict enriched receptor-ligand interactions between subpopulations in decidualizing assembloids (Efremova et al., 2020, Vento-Tormo et al., 2018). Significance was set at $P < 0.05$. Annotated tyrosine kinase interactions were curated manually.

Co-culture of human blastocyst and endometrial assembloids

Prior to co-culture, decidualised assembloids were washed in PBS and medium was replaced with embryo medium (Supplementary Table 1). Assembloids were lightly punctured with a needle to create a small pocket, to enable one re-expanded day 5 human blastocyst to be co-cultured per assembloid. The plate was transferred to a pre-warmed and gassed (humidified 5% CO_2 in air) environment chamber placed on an automated X-Y stage (EVOS® FL Auto Imaging System with onstage incubator) for time-lapse imaging. Brightfield images were captured every 60 minutes over 72 hours. Captured images were converted into videos using ImageJ.

For fixation, assembloid co-cultures were removed from culture wells and transferred into tubes. Samples were washed in PBS and fixed in 10% neutral buffered formalin in the tube for 15 minutes, then washed three times with PBS. Assembloids were permeabilised for 30 minutes in PBS containing 0.3% Triton X-100 and 0.1 M glycine for 30 minutes at room temperature. Samples were incubated overnight at 4°C in primary antibodies diluted in PBS containing 10% FBS, 2% bovine serum albumin (BSA), and 0.1% Tween-20. Samples were then washed in PBS (0.1% Tween-20) and incubated for 2 hours at room temperature protected from light in fluorescently conjugated Alexa Fluor secondary antibodies 1:500 (ThermoFisher Scientific) and DAPI (D3571, ThermoFisher Scientific, dilution 1/500), diluted in PBS containing 10% FBS, 2% BSA, and 0.1% Tween-20. Samples were imaged on a Leica SP8 confocal microscope using a ×25 water objective, with a 0.6 µm z-step and 2× line averaging.

Statistical analysis

649 Data were analysed using GraphPad Prism. For paired, non-parametric significance testing
650 between multiple groups, the Friedman test and Dunn's multiple comparisons *post hoc* test
651 were performed. Only values of $P < 0.05$ were considered statistically significant.

Acknowledgements

We are grateful to the women and couples who participated in this research. We are indebted to Dr. Siobhan Quenby and all the staff in the Centre for Reproductive Medicine and Biomedical Research Unit, University Hospitals Coventry and Warwickshire National Health Service Trust, for facilitating sample collection. This work was supported by a Wellcome Trust Investigator Award to J.J.B (212233/Z/18/Z). T.M.R. was supported by the MRC Doctoral Training Partnership (MR/N014294/1) and a fellowship from Warwick-Wellcome Trust Translational Partnership initiative.

References

ABBAS, Y., CARNICER-LOMBARTE, A., GARDNER, L., THOMAS, J., BROSENS, J. J., MOFFETT, A., SHARKEY, A. M., FRANZE, K., BURTON, G. J. & OYEN, M. L. 2019. Tissue stiffness at the human maternal-fetal interface. *Hum Reprod,* 34**,** 1999-2008.

ACOSTA, J. C., O'LOGHLEN, A., BANITO, A., GUIJARRO, M. V., AUGERT, A., RAGUZ, S., FUMAGALLI, M., DA COSTA, M., BROWN, C., POPOV, N., TAKATSU, Y., MELAMED, J., D'ADDA DI FAGAGNA, F., BERNARD, D., HERNANDO, E. & GIL, J. 2008. Chemokine signaling via the CXCR2 receptor reinforces senescence. *Cell,* 133**,** 1006-18.

APLIN, J. D., CHARLTON, A. K. & AYAD, S. 1988. An immunohistochemical study of human endometrial extracellular matrix during the menstrual cycle and first trimester of pregnancy. *Cell and Tissue Research,* 253**,** 231-240.

APLIN, J. D. & JONES, C. J. P. 1989. Extracellular Matrix in Endometrium and Decidua. *In:* GENBAČEV, O., KLOPPER, A. & BEACONSFIELD, R. (eds.) *Placenta as a Model and a Source*. Boston, MA: Springer US.

APLIN, J. D., MYERS, J. E., TIMMS, K. & WESTWOOD, M. 2020. Tracking placental development in health and disease. *Nat Rev Endocrinol,* 16**,** 479-494.

ASHBURNER, M., BALL, C. A., BLAKE, J. A., BOTSTEIN, D., BUTLER, H., CHERRY, J. M., DAVIS, A. P., DOLINSKI, K., DWIGHT, S. S., EPPIG, J. T., HARRIS, M. A., HILL, D. P., ISSEL-TARVER, L., KASARSKIS, A., LEWIS, S., MATESE, J. C., RICHARDSON, J. E., RINGWALD, M., RUBIN, G. M. & SHERLOCK, G. 2000. Gene ontology: tool for the unification of biology. The Gene Ontology Consortium. *Nat Genet,* 25**,** 25-9.

BAGLEY, B. 2019. *Collagen Gelation Kinetics and Shear Modulus [White paper].* [Online]. Advanced Biomatrix. Available: https://advancedbiomatrix.com/3d-collagen-hydrogel-stiffness.html [Accessed 01/10/2020].

BARROS, F. S., BROSENS, J. J. & BRIGHTON, P. J. 2016. Isolation and Primary Culture of Various Cell Types from Whole Human Endometrial Biopsies. *Bio-protocol,* 6**,** e2028.

BASISTY, N., KALE, A., JEON, O. H., KUEHNEMANN, C., PAYNE, T., RAO, C., HOLTZ, A., SHAH, S., SHARMA, V., FERRUCCI, L., CAMPISI, J. & SCHILLING, B. 2020. A proteomic atlas of senescence-associated secretomes for aging biomarker development. *PLoS Biol,* 18**,** e3000599.

BERKHOUT, R. P., KEIJSER, R., REPPING, S., LAMBALK, C. B., AFINK, G. B., MASTENBROEK, S. & HAMER, G. 2020a. High-quality human preimplantation embryos stimulate endometrial stromal cell migration via secretion of microRNA hsa-miR-320a. *Hum Reprod,* 35**,** 1797-1807.

BERKHOUT, R. P., LAMBALK, C. B., REPPING, S., HAMER, G. & MASTENBROEK, S. 2020b. Premature expression of the decidualization marker prolactin is associated with repeated implantation failure. *Gynecol Endocrinol,* 36**,** 360-364.

BIAN, Y., GAO, G., ZHANG, Q., QIAN, H., YU, L., YAO, N., QIAN, J., LIU, B. & QIAN, X. 2019. KCNQ1OT1/miR-217/ZEB1 feedback loop facilitates cell migration and epithelial-mesenchymal transition in colorectal cancer. *Cancer Biology & Therapy,* 20**,** 886-896.

BIRCH, J. & GIL, J. 2020. Senescence and the SASP: many therapeutic avenues. *Genes Dev,* 34**,** 1565-1576.

BORETTO, M., COX, B., NOBEN, M., HENDRIKS, N., FASSBENDER, A., ROOSE, H., AMANT, F., TIMMERMAN, D., TOMASSETTI, C., VANHIE, A., MEULEMAN, C., FERRANTE, M. & VANKELECOM, H. 2017. Development of organoids from mouse and human

endometrium showing endometrial epithelium physiology and long-term expandability. *Development,* 144**,** 1775-1786.

BRIGHTON, P. J., MARUYAMA, Y., FISHWICK, K., VRLJICAK, P., TEWARY, S., FUJIHARA, R., MUTER, J., LUCAS, E. S., YAMADA, T., WOODS, L., LUCCIOLA, R., HOU LEE, Y., TAKEDA, S., OTT, S., HEMBERGER, M., QUENBY, S. & BROSENS, J. J. 2017. Clearance of senescent decidual cells by uterine natural killer cells in cycling human endometrium. *Elife,* 6.

BROSENS, J. J., HAYASHI, N. & WHITE, J. O. 1999. Progesterone receptor regulates decidual prolactin expression in differentiating human endometrial stromal cells. *Endocrinology,* 140**,** 4809-20.

BURTON, G. J., CINDROVA-DAVIES, T. & TURCO, M. Y. 2020. Review: Histotrophic nutrition and the placental-endometrial dialogue during human early pregnancy. *Placenta,* 102**,** 21-26.

CHAVAN, A. R., GRIFFITH, O. W., STADTMAUER, D., MAZIARZ, J., PAVLICEV, M., FISHMAN, R., KOREN, L., ROMERO, R. & WAGNER, G. P. 2020. Evolution of embryo implantation was enabled by the origin of decidual stromal cells in eutherian mammals. *Mol Biol Evol*.

CHEN, Y., LI, J., XIAO, J.-K., XIAO, L., XU, B.-W. & LI, C. 2021. The lncRNA NEAT1 promotes the epithelial-mesenchymal transition and metastasis of osteosarcoma cells by sponging miR-483 to upregulate STAT3 expression. *Cancer Cell International,* 21**,** 90.

CHRISTIAN, M., MARANGOS, P., MAK, I., MCVEY, J., BARKER, F., WHITE, J. & BROSENS, J. J. 2001. Interferon-gamma modulates prolactin and tissue factor expression in differentiating human endometrial stromal cells. *Endocrinology,* 142**,** 3142-51.

CORDA, G. & SALA, A. 2017. Non-canonical WNT/PCP signalling in cancer: Fzd6 takes centre stage. *Oncogenesis,* 6**,** e364.

COREY, S. J., DOMBROSKY-FERLAN, P. M., ZUO, S., KROHN, E., DONNENBERG, A. D., ZORICH, P., ROMERO, G., TAKATA, M. & KUROSAKI, T. 1998. Requirement of Src kinase Lyn for induction of DNA synthesis by granulocyte colony-stimulating factor. *J Biol Chem,* 273**,** 3230-5.

CUI, X., WANG, H., LI, Y., CHEN, T., LIU, S. & YAN, Q. 2020. Epiregulin promotes trophoblast epithelial-mesenchymal transition through poFUT1 and O-fucosylation by poFUT1 on uPA. *Cell Prolif,* 53**,** e12745.

DALLENBACH-HELLWEG, G. 1981. The Normal Histology of the Endometrium. *Histopathology of the Endometrium.* Berlin, Heidelberg.: Springer.

DIAZ-GIMENO, P., HORCAJADAS, J. A., MARTINEZ-CONEJERO, J. A., ESTEBAN, F. J., ALAMA, P., PELLICER, A. & SIMON, C. 2011. A genomic diagnostic tool for human endometrial receptivity based on the transcriptomic signature. *Fertil Steril,* 95**,** 50-60, 60 e1-15.

DIMITRIADIS, E., MENKHORST, E., SAITO, S., KUTTEH, W. H. & BROSENS, J. J. 2020. Recurrent pregnancy loss. *Nat Rev Dis Primers,* 6**,** 98.

DINIZ-DA-COSTA, M., KONG, C.-S., FISHWICK, K. J., RAWLINGS, T., BRIGHTON, P. J., HAWKES, A., ODENDAAL, J., QUENBY, S., OTT, S., LUCAS, E. S., VRLJICAK, P. & BROSENS, J. J. In press. Characterization of highly proliferative decidual precursor cells during the window of implantation in human endometrium. *Stem Cells*.

EFREMOVA, M., VENTO-TORMO, M., TEICHMANN, S. A. & VENTO-TORMO, R. 2020. CellPhoneDB: inferring cell-cell communication from combined expression of multi-subunit ligand-receptor complexes. *Nat Protoc,* 15**,** 1484-1506.

ELZI, D. J., LAI, Y., SONG, M., HAKALA, K., WEINTRAUB, S. T. & SHIIO, Y. 2012. Plasminogen activator inhibitor 1--insulin-like growth factor binding protein 3 cascade regulates stress-induced senescence. *Proc Natl Acad Sci U S A,* 109**,** 12052-7.

ERKENBRACK, E. M., MAZIARZ, J. D., GRIFFITH, O. W., LIANG, C., CHAVAN, A. R., NNAMANI, M. C. & WAGNER, G. P. 2018. The mammalian decidual cell evolved from a cellular stress response. *PLoS Biol,* 16**,** e2005594.

FERENCZY, A., BERTRAND, G. & GELFAND, M. M. 1979. Proliferation kinetics of human endometrium during the normal menstrual cycle. *Am J Obstet Gynecol,* 133**,** 859-67.

GELLERSEN, B. & BROSENS, J. J. 2014. Cyclic decidualization of the human endometrium in reproductive health and failure. *Endocr Rev,* 35**,** 851-905.

GELLERSEN, B., REIMANN, K., SAMALECOS, A., AUPERS, S. & BAMBERGER, A. M. 2010. Invasiveness of human endometrial stromal cells is promoted by decidualization and by trophoblast-derived signals. *Hum Reprod,* 25**,** 862-73.

GREWAL, S., CARVER, J. G., RIDLEY, A. J. & MARDON, H. J. 2008. Implantation of the human embryo requires Rac1-dependent endometrial stromal cell migration. *Proc Natl Acad Sci U S A,* 105**,** 16189-94.

HAIDER, S., GAMPERL, M., BURKARD, T. R., KUNIHS, V., KAINDL, U., JUNTTILA, S., FIALA, C., SCHMIDT, K., MENDJAN, S., KNOFLER, M. & LATOS, P. A. 2019. Estrogen Signaling Drives Ciliogenesis in Human Endometrial Organoids. *Endocrinology,* 160**,** 2282-2297.

HO, K. H., CHEN, P. H., CHOU, C. M., SHIH, C. M., LEE, Y. T., CHENG, C. H. & CHEN, K. C. 2020. A Key Role of DNA Damage-Inducible Transcript 4 (DDIT4) Connects Autophagy and GLUT3-Mediated Stemness To Desensitize Temozolomide Efficacy in Glioblastomas. *Neurotherapeutics,* 17**,** 1212-1227.

HUPPERTZ, B. 2019. Traditional and New Routes of Trophoblast Invasion and Their Implications for Pregnancy Diseases. *Int J Mol Sci,* 21.

IWAHASHI, M., MURAGAKI, Y., OOSHIMA, A., YAMOTO, M. & NAKANO, R. 1996. Alterations in distribution and composition of the extracellular matrix during decidualization of the human endometrium. *J Reprod Fertil,* 108**,** 147-55.

JABBOUR, H. N., KELLY, R. W., FRASER, H. M. & CRITCHLEY, H. O. 2006. Endocrine regulation of menstruation. *Endocr Rev,* 27**,** 17-46.

KASIUS, A., SMIT, J. G., TORRANCE, H. L., EIJKEMANS, M. J., MOL, B. W., OPMEER, B. C. & BROEKMANS, F. J. 2014. Endometrial thickness and pregnancy rates after IVF: a systematic review and meta-analysis. *Hum Reprod Update,* 20**,** 530-41.

KIM, K. M., NOH, J. H., BODOGAI, M., MARTINDALE, J. L., YANG, X., INDIG, F. E., BASU, S. K., OHNUMA, K., MORIMOTO, C., JOHNSON, P. F., BIRAGYN, A., ABDELMOHSEN, K. & GOROSPE, M. 2017. Identification of senescent cell surface targetable protein DPP4. *Genes Dev,* 31**,** 1529-1534.

KOLER, M., ACHACHE, H., TSAFRIR, A., SMITH, Y., REVEL, A. & REICH, R. 2009. Disrupted gene pattern in patients with repeated in vitro fertilization (IVF) failure. *Hum Reprod,* 24**,** 2541-8.

KONG, C.-S., ORDOÑEZ, A. A., TURNER, S., TREMAINE, T., MUTER, J., LUCAS, E. S., SALISBURY, E., VASSENA, R., FOULADI-NASHTA, A. A., TISCORNIA, G., HARTSHORNE, G., BROSENS, J. J. & BRIGHTON, P. J. In press. Involvement of uterine natural killer cells in the natural selection of human embryos at implantation. *FASEB J*.

KOOT, Y. E., VAN HOOFF, S. R., BOOMSMA, C. M., VAN LEENEN, D., GROOT KOERKAMP, M. J., GODDIJN, M., EIJKEMANS, M. J., FAUSER, B. C., HOLSTEGE, F. C. & MACKLON, N. S.

2016. An endometrial gene expression signature accurately predicts recurrent implantation failure after IVF. *Sci Rep,* 6**,** 19411.

KUILMAN, T., MICHALOGLOU, C., VREDEVELD, L. C., DOUMA, S., VAN DOORN, R., DESMET, C. J., AARDEN, L. A., MOOI, W. J. & PEEPER, D. S. 2008. Oncogene-induced senescence relayed by an interleukin-dependent inflammatory network. *Cell,* 133**,** 1019-31.

LEE, C. L., LAM, K. K., VIJAYAN, M., KOISTINEN, H., SEPPALA, M., NG, E. H., YEUNG, W. S. & CHIU, P. C. 2016. The Pleiotropic Effect of Glycodelin-A in Early Pregnancy. *Am J Reprod Immunol,* 75**,** 290-7.

LUCAS, E. S., DYER, N. P., MURAKAMI, K., LEE, Y. H., CHAN, Y. W., GRIMALDI, G., MUTER, J., BRIGHTON, P. J., MOORE, J. D., PATEL, G., CHAN, J. K., TAKEDA, S., LAM, E. W., QUENBY, S., OTT, S. & BROSENS, J. J. 2016. Loss of Endometrial Plasticity in Recurrent Pregnancy Loss. *Stem Cells,* 34**,** 346-56.

LUCAS, E. S., VRLJICAK, P., MUTER, J., DINIZ-DA-COSTA, M. M., BRIGHTON, P. J., KONG, C. S., LIPECKI, J., FISHWICK, K. J., ODENDAAL, J., EWINGTON, L. J., QUENBY, S., OTT, S. & BROSENS, J. J. 2020. Recurrent pregnancy loss is associated with a pro-senescent decidual response during the peri-implantation window. *Commun Biol,* 3**,** 37.

MACKLON, N. 2017. Recurrent implantation failure is a pathology with a specific transcriptomic signature. *Fertil Steril,* 108**,** 9-14.

MACOSKO, E. Z., BASU, A., SATIJA, R., NEMESH, J., SHEKHAR, K., GOLDMAN, M., TIROSH, I., BIALAS, A. R., KAMITAKI, N., MARTERSTECK, E. M., TROMBETTA, J. J., WEITZ, D. A., SANES, J. R., SHALEK, A. K., REGEV, A. & MCCARROLL, S. A. 2015. Highly Parallel Genome-wide Expression Profiling of Individual Cells Using Nanoliter Droplets. *Cell,* 161**,** 1202-1214.

MARINIC, M., MIKA, K., CHIGURUPATI, S. & LYNCH, V. J. 2021. Evolutionary transcriptomics implicates HAND2 in the origins of implantation and regulation of gestation length. *Elife,* 10.

MI, H., MURUGANUJAN, A., CASAGRANDE, J. T. & THOMAS, P. D. 2013. Large-scale gene function analysis with the PANTHER classification system. *Nat Protoc,* 8**,** 1551-66.

MILLER, W. P., SUNILKUMAR, S., GIORDANO, J. F., TORO, A. L., BARBER, A. J. & DENNIS, M. D. 2020. The stress response protein REDD1 promotes diabetes-induced oxidative stress in the retina by Keap1-independent Nrf2 degradation. *J Biol Chem,* 295**,** 7350-7361.

MOSER, G., GAUSTER, M., ORENDI, K., GLASNER, A., THEUERKAUF, R. & HUPPERTZ, B. 2010. Endoglandular trophoblast, an alternative route of trophoblast invasion? Analysis with novel confrontation co-culture models. *Hum Reprod,* 25**,** 1127-36.

MUNOZ-ESPIN, D. & SERRANO, M. 2014. Cellular senescence: from physiology to pathology. *Nat Rev Mol Cell Biol,* 15**,** 482-96.

OEFNER, C. M., SHARKEY, A., GARDNER, L., CRITCHLEY, H., OYEN, M. & MOFFETT, A. 2015. Collagen type IV at the fetal-maternal interface. *Placenta,* 36**,** 59-68.

OWUSU-AKYAW, A., KRISHNAMOORTHY, K., GOLDSMITH, L. T. & MORELLI, S. S. 2019. The role of mesenchymal-epithelial transition in endometrial function. *Hum Reprod Update,* 25**,** 114-133.

OZAKI, R., KURODA, K., IKEMOTO, Y., OCHIAI, A., MATSUMOTO, A., KUMAKIRI, J., KITADE, M., ITAKURA, A., MUTER, J., BROSENS, J. J. & TAKEDA, S. 2017. Reprogramming of the retinoic acid pathway in decidualizing human endometrial stromal cells. *PLoS One,* 12**,** e0173035.

PATTERSON, A. L., ZHANG, L., ARANGO, N. A., TEIXEIRA, J. & PRU, J. K. 2013. Mesenchymal-to-epithelial transition contributes to endometrial regeneration following natural and artificial decidualization. *Stem Cells Dev,* 22**,** 964-74.

PFAFFL, M. W. 2001. A new mathematical model for relative quantification in real-time RT-PCR. *Nucleic Acids Res,* 29**,** e45.

POLANSKI, L. T., BAUMGARTEN, M. N., QUENBY, S., BROSENS, J., CAMPBELL, B. K. & RAINE-FENNING, N. J. 2014. What exactly do we mean by 'recurrent implantation failure'? A systematic review and opinion. *Reprod Biomed Online,* 28**,** 409-23.

RAINE-FENNING, N. J., CAMPBELL, B. K., CLEWES, J. S., KENDALL, N. R. & JOHNSON, I. R. 2004. Defining endometrial growth during the menstrual cycle with three-dimensional ultrasound. *BJOG,* 111**,** 944-9.

RAJAGOPALAN, S. & LONG, E. O. 2012. Cellular senescence induced by CD158d reprograms natural killer cells to promote vascular remodeling. *Proc Natl Acad Sci U S A,* 109**,** 20596-601.

RUAN, Y. C., GUO, J. H., LIU, X., ZHANG, R., TSANG, L. L., DONG, J. D., CHEN, H., YU, M. K., JIANG, X., ZHANG, X. H., FOK, K. L., CHUNG, Y. W., HUANG, H., ZHOU, W. L. & CHAN, H. C. 2012. Activation of the epithelial Na+ channel triggers prostaglandin E(2) release and production required for embryo implantation. *Nat Med,* 18**,** 1112-7.

SALKER, M. S., NAUTIYAL, J., STEEL, J. H., WEBSTER, Z., SUCUROVIC, S., NICOU, M., SINGH, Y., LUCAS, E. S., MURAKAMI, K., CHAN, Y. W., JAMES, S., ABDALLAH, Y., CHRISTIAN, M., CROY, B. A., MULAC-JERICEVIC, B., QUENBY, S. & BROSENS, J. J. 2012. Disordered IL-33/ST2 activation in decidualizing stromal cells prolongs uterine receptivity in women with recurrent pregnancy loss. *PLoS One,* 7**,** e52252.

STUART, T., BUTLER, A., HOFFMAN, P., HAFEMEISTER, C., PAPALEXI, E., MAUCK, W. M., 3RD, HAO, Y., STOECKIUS, M., SMIBERT, P. & SATIJA, R. 2019. Comprehensive Integration of Single-Cell Data. *Cell,* 177**,** 1888-1902 e21.

TABIBZADEH, S. 1991. Induction of HLA-DR expression in endometrial epithelial cells by endometrial T-cells: potential regulatory role of endometrial T-cells in vivo. *J Clin Endocrinol Metab,* 73**,** 1352-9.

TABIBZADEH, S., SUN, X. Z., KONG, Q. F., KASNIC, G., MILLER, J. & SATYASWAROOP, P. G. 1993. Induction of a polarized micro-environment by human T cells and interferon-gamma in three-dimensional spheroid cultures of human endometrial epithelial cells. *Hum Reprod,* 8**,** 182-92.

TEWARY, S., LUCAS, E. S., FUJIHARA, R., KIMANI, P. K., POLANCO, A., BRIGHTON, P. J., MUTER, J., FISHWICK, K. J., DA COSTA, M., EWINGTON, L. J., LACEY, L., TAKEDA, S., BROSENS, J. J. & QUENBY, S. 2020. Impact of sitagliptin on endometrial mesenchymal stem-like progenitor cells: A randomised, double-blind placebo-controlled feasibility trial. *EBioMedicine,* 51**,** 102597.

THE GENE ONTOLOGY, C. 2019. The Gene Ontology Resource: 20 years and still GOing strong. *Nucleic Acids Res,* 47**,** D330-D338.

TICCONI, C., PIETROPOLLI, A., D'IPPOLITO, S., CHIARAMONTE, C., PICCIONE, E., SCAMBIA, G. & DI SIMONE, N. 2020. Time-to-Pregnancy in Women with Unexplained Recurrent Pregnancy Loss: A Controlled Study. *Reprod Sci,* 27**,** 1121-1128.

TURCO, M. Y., GARDNER, L., HUGHES, J., CINDROVA-DAVIES, T., GOMEZ, M. J., FARRELL, L., HOLLINSHEAD, M., MARSH, S. G. E., BROSENS, J. J., CRITCHLEY, H. O., SIMONS, B. D., HEMBERGER, M., KOO, B. K., MOFFETT, A. & BURTON, G. J. 2017. Long-term,

hormone-responsive organoid cultures of human endometrium in a chemically defined medium. *Nat Cell Biol,* 19**,** 568-577.

VAN DER VOORT, R., TAHER, T. E., WIELENGA, V. J., SPAARGAREN, M., PREVO, R., SMIT, L., DAVID, G., HARTMANN, G., GHERARDI, E. & PALS, S. T. 1999. Heparan sulfate-modified CD44 promotes hepatocyte growth factor/scatter factor-induced signal transduction through the receptor tyrosine kinase c-Met. *J Biol Chem,* 274**,** 6499-506.

VAN DEURSEN, J. M. 2014. The role of senescent cells in ageing. *Nature,* 509**,** 439-46.

VENTO-TORMO, R., EFREMOVA, M., BOTTING, R. A., TURCO, M. Y., VENTO-TORMO, M., MEYER, K. B., PARK, J. E., STEPHENSON, E., POLANSKI, K., GONCALVES, A., GARDNER, L., HOLMQVIST, S., HENRIKSSON, J., ZOU, A., SHARKEY, A. M., MILLAR, B., INNES, B., WOOD, L., WILBREY-CLARK, A., PAYNE, R. P., IVARSSON, M. A., LISGO, S., FILBY, A., ROWITCH, D. H., BULMER, J. N., WRIGHT, G. J., STUBBINGTON, M. J. T., HANIFFA, M., MOFFETT, A. & TEICHMANN, S. A. 2018. Single-cell reconstruction of the early maternal-fetal interface in humans. *Nature,* 563**,** 347-353.

WEIMAR, C. H., KAVELAARS, A., BROSENS, J. J., GELLERSEN, B., DE VREEDEN-ELBERTSE, J. M., HEIJNEN, C. J. & MACKLON, N. S. 2012. Endometrial stromal cells of women with recurrent miscarriage fail to discriminate between high- and low-quality human embryos. *PLoS One,* 7**,** e41424.

YU, Y., FANG, L., WANG, S., LI, Y., GUO, Y. & SUN, Y. P. 2019. Amphiregulin promotes trophoblast invasion and increases MMP9/TIMP1 ratio through ERK1/2 and Akt signal pathways. *Life Sci,* 236**,** 116899.

ZHENG, J., QU, D., WANG, C., DING, L. & ZHOU, W. 2020. Involvement of CXCL12/CXCR4 in the motility of human first-trimester endometrial epithelial cells through an autocrine mechanism by activating PI3K/AKT signaling. *BMC Pregnancy Childbirth,* 20**,** 87.

ZHOU, Q., YAN, G., DING, L., LIU, J., YU, X., KONG, S., ZHANG, M., WANG, Z., LIU, Y., JIANG, Y., KONG, N., SUN, J. & SUN, H. 2019. EHD1 impairs decidualization by regulating the Wnt4/beta-catenin signaling pathway in recurrent implantation failure. *EBioMedicine,* 50**,** 343-354.

ZHU, Y., TCHKONIA, T., PIRTSKHALAVA, T., GOWER, A. C., DING, H., GIORGADZE, N., PALMER, A. K., IKENO, Y., HUBBARD, G. B., LENBURG, M., O'HARA, S. P., LARUSSO, N. F., MILLER, J. D., ROOS, C. M., VERZOSA, G. C., LEBRASSEUR, N. K., WREN, J. D., FARR, J. N., KHOSLA, S., STOUT, M. B., MCGOWAN, S. J., FUHRMANN-STROISSNIGG, H., GURKAR, A. U., ZHAO, J., COLANGELO, D., DORRONSORO, A., LING, Y. Y., BARGHOUTHY, A. S., NAVARRO, D. C., SANO, T., ROBBINS, P. D., NIEDERNHOFER, L. J. & KIRKLAND, J. L. 2015. The Achilles' heel of senescent cells: from transcriptome to senolytic drugs. *Aging Cell,* 14**,** 644-58.

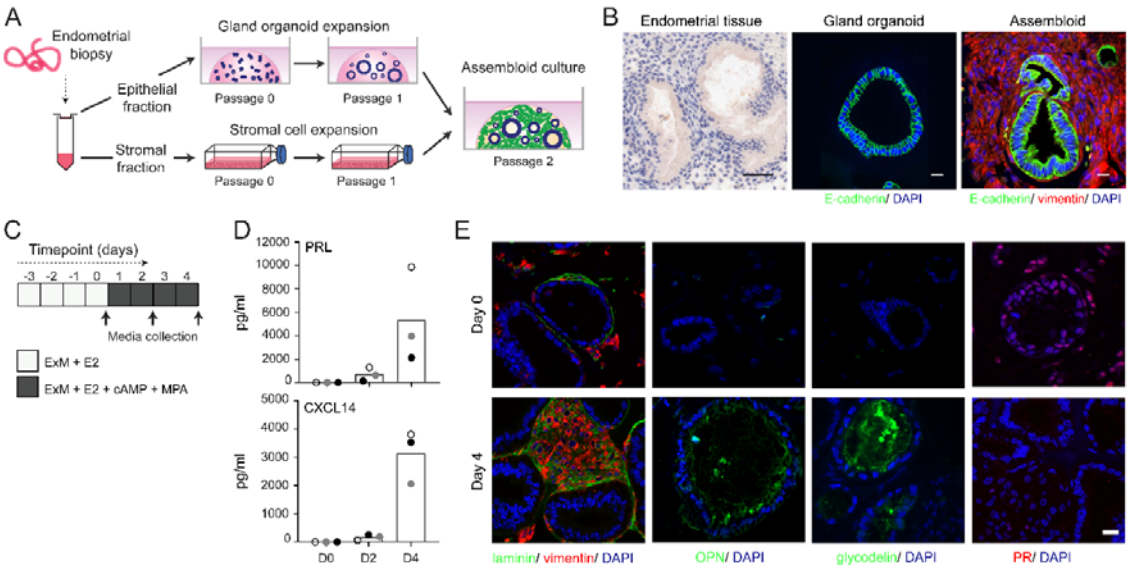

Figure 1: Establishment of endometrial assembloids.

(A) Schematic for establishing endometrial assembloids. (B) Structural appearance of hematoxylin and eosin stained secretory endometrium, E-cadherin labelled gland organoids, and E-cadherin and vimentin stained endometrial assembloids. Scale bar = 50 µm. (C) Schematic summary of experimental design. (D) Secreted levels of PRL and CXCL14 were measured by ELISA in spent medium at the indicated timepoints. Data points are coloured to indicate secretion in assembloids established from different endometrial biopsies (n=3). (E) Representative immunofluorescence labelling of laminin and vimentin, progesterone receptor (PR), glycodelin and osteopontin (OPN) in undifferentiated (Day 0, top panels) and decidualised (Day 4; bottom panels) assembloids. Nuclei were counterstained with DAPI. Scale bar = 50 µm. ELISA data in Panel B are available in Figure 1-Source Data 1.

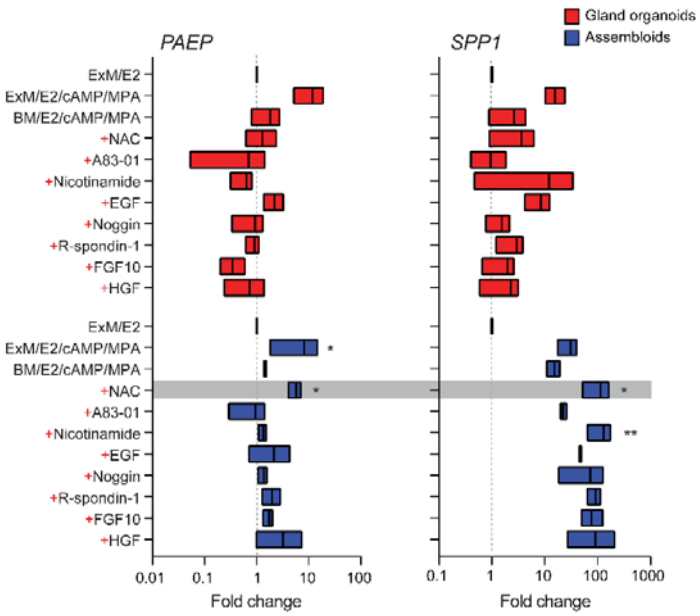

Figure 2: Characterisation of a minimal differentiation medium for endometrial assembloids. Parallel gland organoids (blue) and assembloids (red) were established from 3 endometrial biopsies and decidualized with 8-bromo-cAMP and MPA for 4 days in either expansion medium (ExM), base medium (BM) or BM with each exogeneous factor added back individually (+). Induction of *PAEP* and *SPP1* was used to monitor the glandular differentiation. The grey bar indicates the composition of the minimal differentiation medium selected for further use (BM supplemented with NAC, E2, cAMP, and MPA). Data are presented as fold-change relative to expression levels in undifferentiated organoids or assembloids cultured in ExM+E2. Bars present minimal, maximal, and median fold-change. * and ** indicate $P < 0.05$ and $P < 0.01$ obtained by Friedman's test for matched samples. Relative expression values for biological replicates are available in Figure 2-Source Data 2.

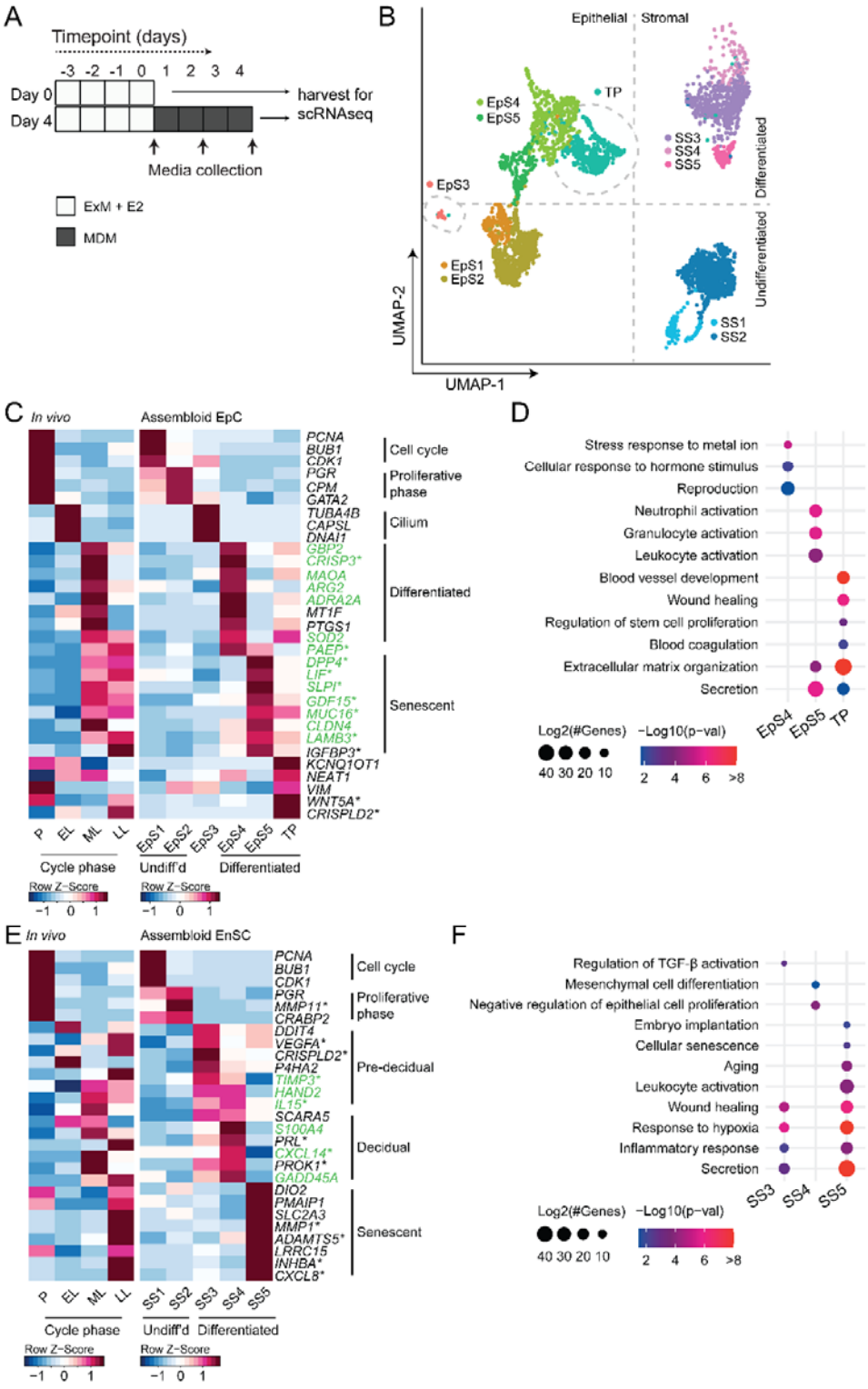

Figure 3: Decidualizing assembloids mimic midluteal endometrium

(A) Schematic overview of experimental design. ExM, expansion medium; MDM, minimal differentiation medium. (B) UMAP visualizing epithelial and stromal subsets (EpS and SS,

respectively) identified by single-cell transcriptomic analysis of undifferentiated and decidualized assembloids. A transitional population (TP) consisting of cells expressing epithelial and stromal markers is also shown. Dotted lines indicate the separation of EpS and SS in UMAP_1 and of undifferentiated and differentiated subpopulations in UMAP_2. (C) Composite heatmaps showing relative expression (Z-scores) of epithelial marker genes across the menstrual cycle *in vivo* and in undifferentiated and decidualized assembloids. Highlighted in green are genes that mark the midluteal window of implantation whereas genes encoding secreted proteins are indicated by *. See also Figure 3-figure supplement 1. (D) Dot plots showing GO terms related to biological processes enriched in different epithelial populations in decidualizing assembloids. The dot size represents the number of genes in each GO term and the colour indicates FDR-corrected *P*-value. (E) Composite heatmaps showing relative expression (Z-scores) of stromal marker genes across the menstrual cycle *in vivo* and in undifferentiated and decidualized assembloids. Highlighted in green are genes that mark the midluteal window of implantation whereas genes encoding secreted proteins are indicated by *. (F) Dot plots showing GO terms related to biological processes enriched in different stromal subpopulations in decidualizing assembloids. See also Figure 3-figure supplements 1, 2 and 3. Complete epithelial subpopulation marker lists can be found in Figure 3-Source Data 1. GO analysis outputs can be found in Figure 3-Source Data 2. Complete stromal subpopulation marker lists can be found in Figure 3-Source Data 3.

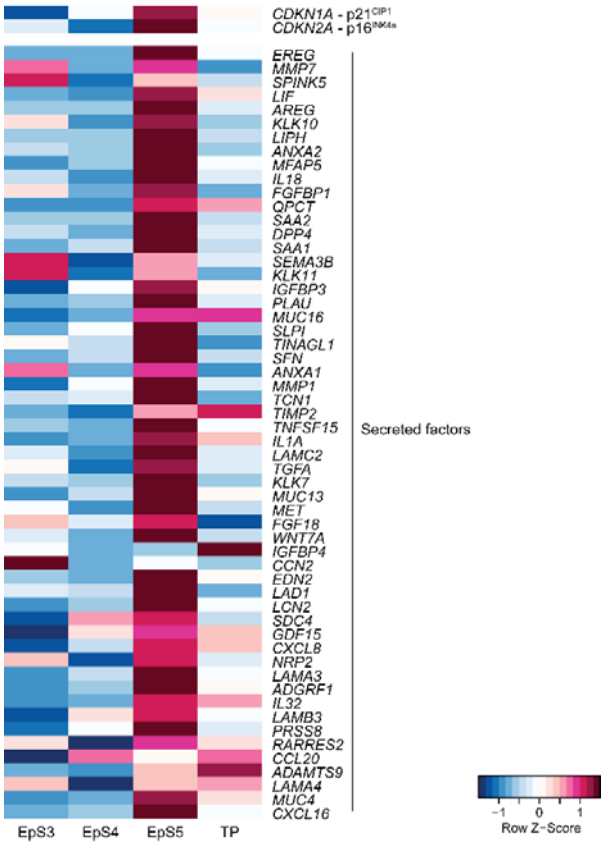

Figure 3–figure supplement 1:

Heatmap showing relative expression (Z-scores) of genes encoding the cyclin-dependent kinase inhibitors $p16^{INK4a}$ and $p21^{CIP1}$ as well as SASP-related genes in epithelial and transitional subpopulations in decidualizing assembloids. Supports Figure 3C.

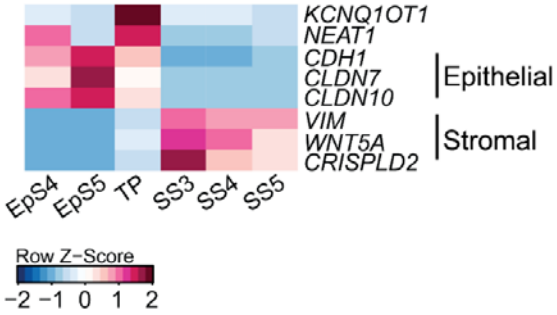

Figure 3–figure supplement 2:

Heatmap showing relative expression (Z-scores) of EMT/MET, epithelial and mesenchymal marker genes in the transitional population (TP), epithelial (EpS4-5) and stromal (SS3-5) subpopulations in decidualizing assembloids. Supports Figure 3C.

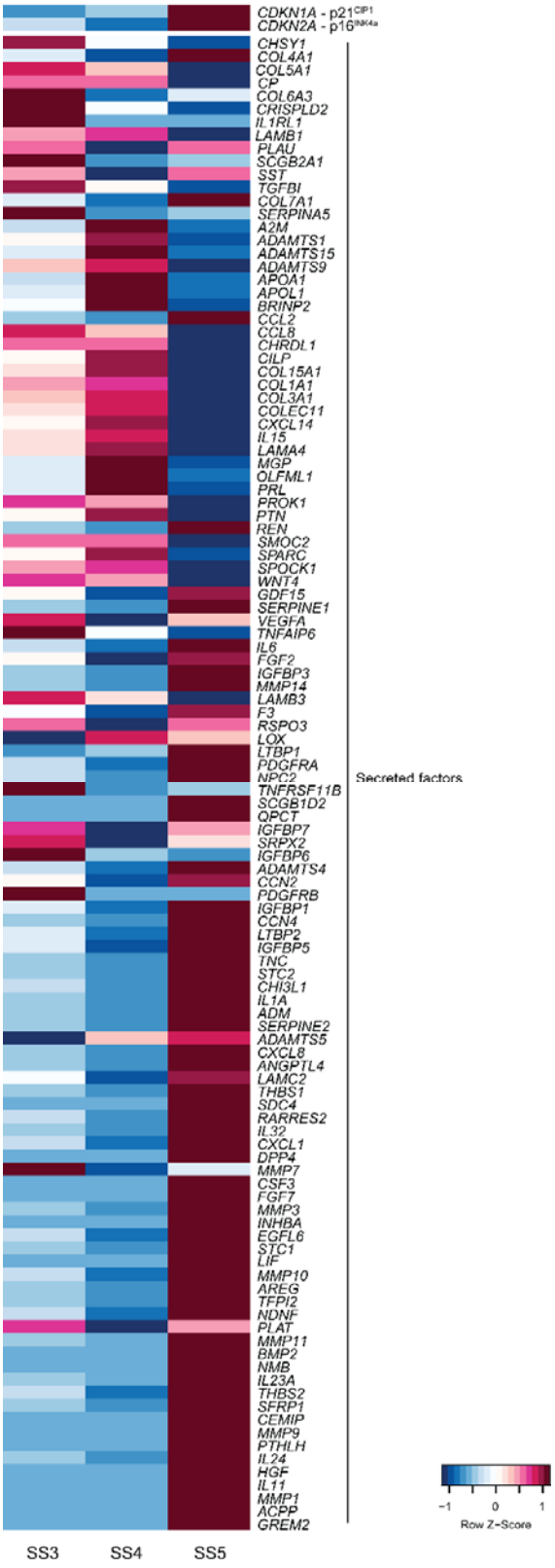

Figure 3–figure supplement 3:

Heatmap showing relative expression (Z-scores) of genes encoding the cyclin-dependent kinase inhibitors $p16^{INK4a}$ and $p21^{CIP1}$ as well as secretory and SASP-related genes in stromal subpopulations (SS3-5) in decidualizing assembloids. Supports Figure 3D.

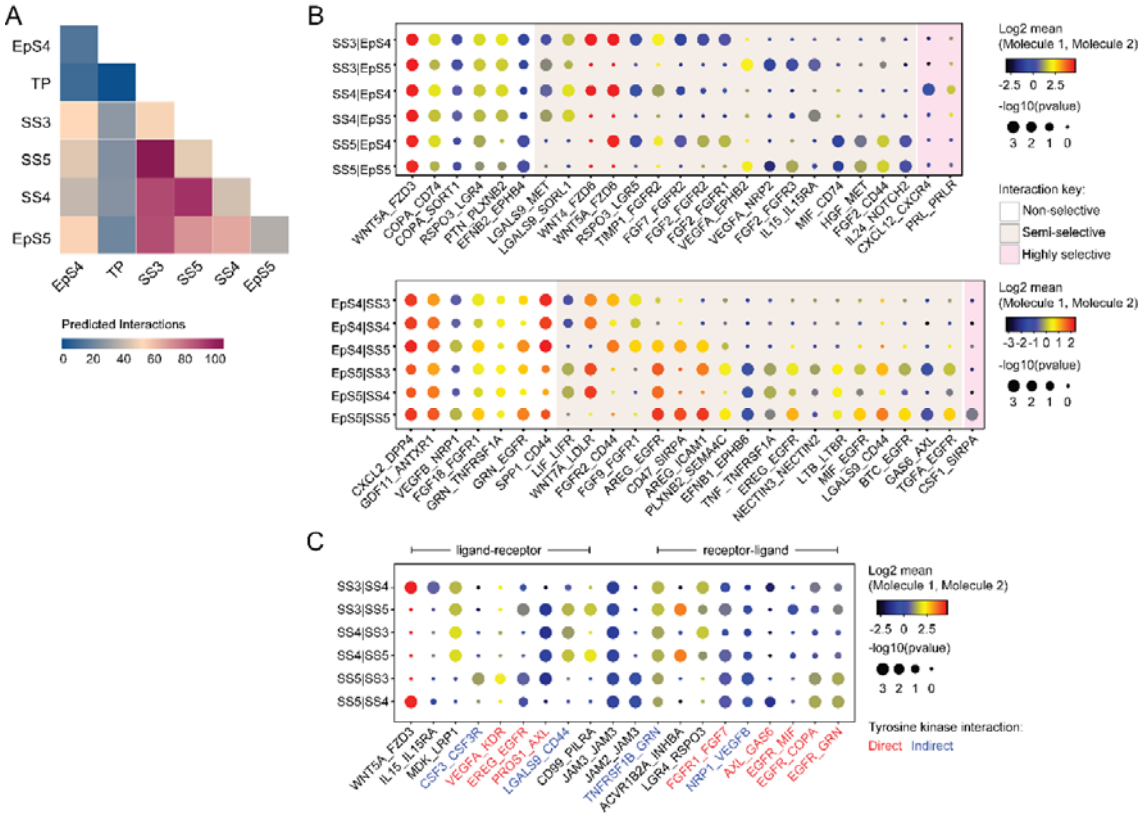

Figure 4: Putative receptor-ligand interactions in decidualizing assembloids

(A) Heatmap showing the total number of cell-cell interactions predicted by CellPhoneDB between different subpopulations in decidualizing assembloids. (B) Dot plots of representative ligand-receptor interactions between SS and EpS (upper panel) and EpS and SS (lower panel) in decidualizing assembloids. Circle size and colour indicate *P*-value and the means of the average expression value of the interacting molecules, respectively. Shaded boxes were used to group putative interactions by level of selectivity. (C) Dot plot of representative ligand-receptor and receptor-ligand interactions between stromal subpopulations in decidualizing assembloids. Direct and indirect tyrosine kinase interactions are indicated by red and blue labels, respectively. Complete tables of predicted ligand-receptor interactions can be found in Figure 4-Source Data 1.

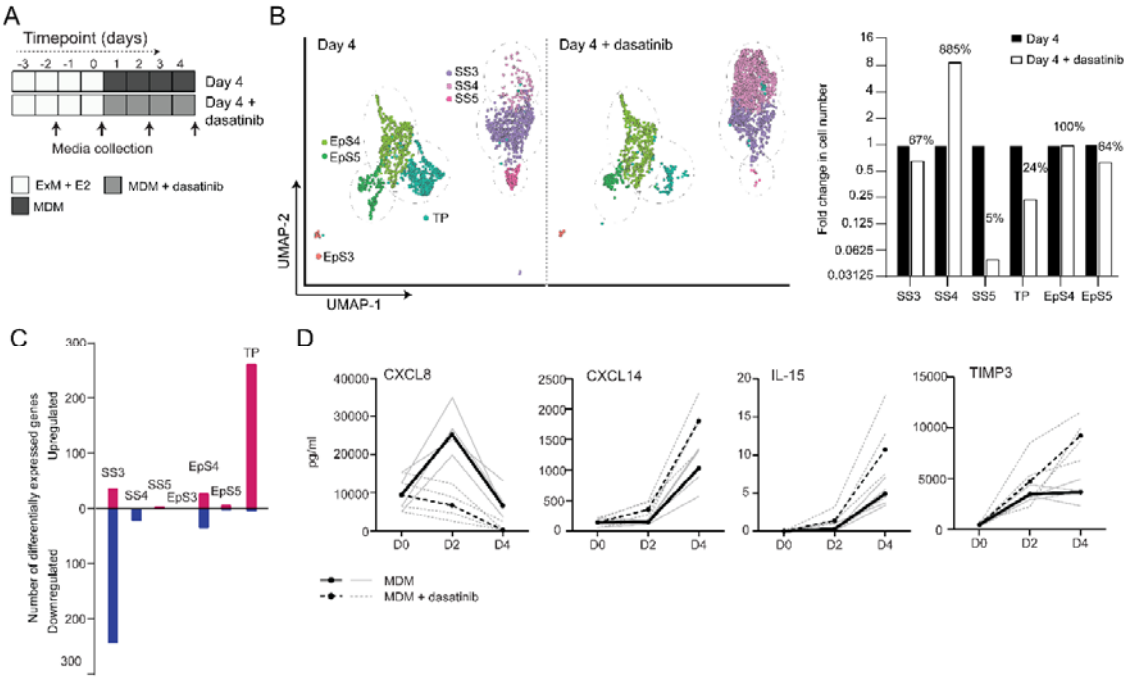

Figure 5: Tyrosine kinase-dependent stress responses determines the fate of decidual cells

(A) Schematic overview of experimental design. ExM, expansion medium; MDM, minimal differentiation medium. (B) UMAP visualisation (left panel) and relative proportions (right panel) of subpopulations in endometrial assembloid decidualized in the presence or absence of dasatinib. (C) Number of differentially expressed genes (DEG) in each subpopulation in response to dasatinib pretreatment. (D) Secreted levels of CXCL8 and decidual cell factors in spent medium from assembloids treated with or without dasatinib. Secreted levels in individual assembloids established from 4 different endometrial assembloids decidualized with or without dasatinib are shown by dotted and solid lines, respectively. Full lists of differentially expressed genes and associated gene ontology analysis can be found in Figure 5-Source Data 1 and 2, respectively. Data used in Panel D are available in Figure 5-Source Data 3

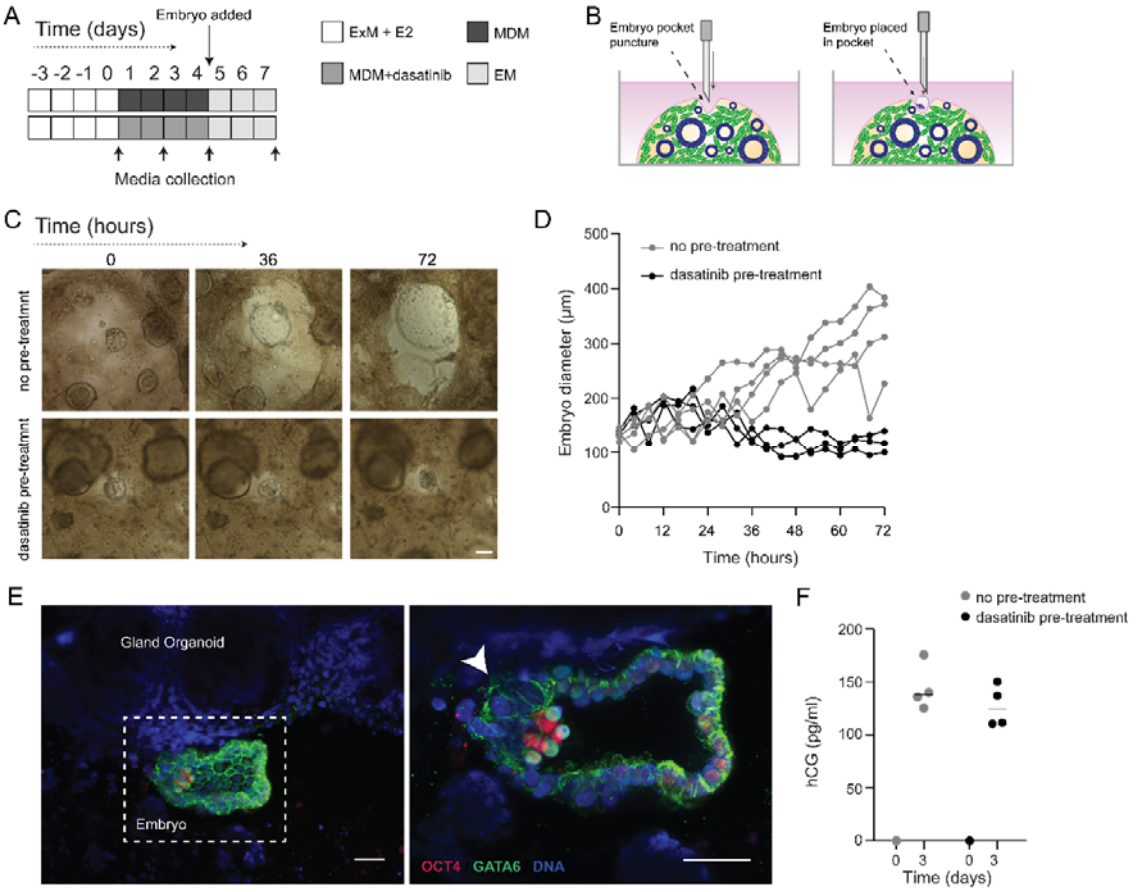

Figure 6: Impact of decidual senescence in assembloids on co-cultured human blastocysts

(A) Diagram showing experimental design. ExM, expansion medium; MDM, minimal differentiation medium; EM, embryo medium. (B) Schematic drawing of co-culture method. (C) Representative time-lapse images of blastocysts embedded in assembloids following decidualization for 96 hours in the absence (upper panels) or presence (lower panels) of dasatinib. See also Figure 6–figure supplement 1. (D) Expansion of embryos over 72 hours when embedded in decidualizing assembloids pre-treated with or without dasatinib. Scale bar = 100 µm. (E) OCT4 and GATA6 immunofluorescence marking the epiblast and hypoblast, respectively, in a blastocyst attached by proliferating polar trophectoderm (arrowhead) to decidual assembloids. Scale bar = 50 µM. (F) Secreted levels of hCG in blastocyst-endometrial assembloid co-cultures. Individual embryo diameter measurements for biological replicates in Panel D are available in Figure 6-Source Data 1. Individual ELISA data used in Panel F are available in Figure 6-Source Data 2.

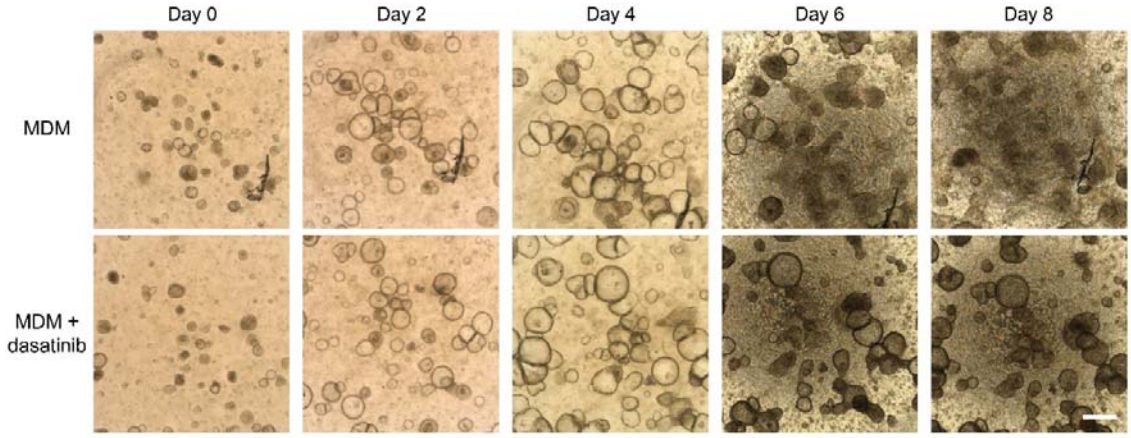

Figure 6–figure supplement 1: dasatinib prevents disintegration of decidualizing assembloids

Time-course images of endometrial assembloids in minimal differentiation medium (MDM) supplemented or not with dasatinib. Scale bar = 50 µm.